PTEP

Prog. Theor. Exp. Phys. **2015**, 053C01 (31 pages)
DOI: 10.1093/ptep/ptv054

Measurement of the muon beam direction and muon flux for the T2K neutrino experiment

K. Suzuki[1,*], S. Aoki[2], A. Ariga[3], T. Ariga[3], F. Bay[3,†], C. Bronner[4], A. Ereditato[3], M. Friend[5], M. Hartz[4,6], T. Hiraki[1], A. K. Ichikawa[1], T. Ishida[5], T. Ishii[5], F. Juget[3,‡], T. Kikawa[1,§], T. Kobayashi[5], H. Kubo[1], K. Matsuoka[1,¶], T. Maruyama[5], A. Minamino[1], A. Murakami[1,%], T. Nakadaira[5], T. Nakaya[1], K. Nakayoshi[5], M. Otani[1,**], Y. Oyama[5], N. Patel[1], C. Pistillo[3], K. Sakashita[5], T. Sekiguchi[5], S. Y. Suzuki[5], S. Tada[5], Y. Yamada[5], K. Yamamoto[7], and M. Yokoyama[8]

[1]*Department of Physics, Kyoto University, Kyoto 606-8502, Japan*
[2]*Kobe University, Kobe, Hyogo 657-8501, Japan*
[3]*Albert Einstein Center for Fundamental Physics, Laboratory for High Energy Physics (LHEP), University of Bern, Bern 3012, Switzerland*
[4]*Kavli Institute for the Physics and Mathematics of the Universe (WPI), Todai Institutes for Advanced Study, University of Tokyo, Kashiwa, Chiba 277-8583, Japan*
[5]*High Energy Accelerator Research Organization (KEK), Tsukuba, Ibaraki 305-0801, Japan*
[6]*TRIUMF, Vancouver, British Columbia, V6T 2A3, Canada*
[7]*Department of Physics, Osaka City University, Osaka 558-8585, Japan*
[8]*Department of Physics, University of Tokyo, Bunkyo, Tokyo 113-0033, Japan*
[*]E-mail: k.suzuki@scphys.kyoto-u.ac.jp

Received November 25, 2014; Revised March 19, 2015; Accepted March 19, 2015; Published May 11, 2015

The Tokai-to-Kamioka (T2K) neutrino experiment measures neutrino oscillations by using an almost pure muon neutrino beam produced at the J-PARC accelerator facility. The T2K muon monitor was installed to measure the direction and stability of the muon beam which is produced in conjunction with the muon neutrino beam. The systematic error in the muon beam direction measurement was estimated, using data and MC simulation, to be 0.28 mrad. During beam operation, the proton beam has been controlled using measurements from the muon monitor and the direction of the neutrino beam has been tuned to within 0.3 mrad with respect to the designed beam-axis. In order to understand the muon beam properties, measurement of the absolute muon yield at the muon monitor was conducted with an emulsion detector. The number of muon tracks was measured to be $(4.06 \pm 0.05 \pm 0.10) \times 10^4$ cm^{-2} normalized with 4×10^{11} protons on target with 250 kA horn operation. The result is in agreement with the prediction, which is corrected based on hadron production data.

Subject Index C32

[†]Present address: Institute for Particle Physics, ETH Zurich, Zurich 8092, Switzerland
[‡]Present address: Institute of Radiation Physics, University Hospital and University of Lausanne, Lausanne 1015, Switzerland
[§]Present address: Research Center for Nuclear Physics, Osaka University, Ibaraki, Osaka 567-0047, Japan
[¶]Present address: Kobayashi-Maskawa Istitute, Nagoya University, Nagoya 464-8602, Japan
[%]Present address: Toshiba Corporation, Kawasaki, Kanagawa 212-0001, Japan
[**]Present address: KEK, Tsukuba, Ibaraki 305-0801, Japan

1. Introduction

The Tokai-to-Kamioka (T2K) experiment [1] is a long baseline neutrino oscillation experiment in Japan. The neutrino oscillation parameters are determined by measuring an accelerator-produced neutrino beam before oscillation with the near detector and near the oscillation maximum with the far detector. T2K began operation in January 2010. Since then, data corresponding to a total of 6.63×10^{20} protons on target (p.o.t.) had been collected as of May 2013.

The T2K muon monitor [2] was installed to monitor the muon beam which is produced together with the neutrino beam from the decay of pions. In an accelerator-based long baseline neutrino experiment, control of the neutrino beam is one of the key items. As we describe later, T2K utilizes the off-axis method whereby the central axis of the beam is intentionally shifted by 2.5° from the direction of the near and far detectors. This method enables us to measure the oscillation parameters with high sensitivity. On the other hand, it requires stringent control of the neutrino beam direction. Thus, it is important to monitor the neutrino beam direction on a spill-by-spill basis with good precision. As the muon monitor is the only detector which can monitor the beam spill-by-spill, our strategy is to monitor the muon beam direction with a precision of 0.3 mrad for every beam spill, in order to better control the neutrino beam for the neutrino oscillation measurement. To accomplish this, it is highly important to evaluate the detector performance. In addition, a direct muon flux measurement would strengthen the strategy to control the neutrino beam based on the muon beam monitoring.

In this paper, we first provide an overview of the T2K experiment, emphasizing the importance of a precise measurement of the muon beam direction in Sect. 2. Section 3 gives an overview of the components of the muon monitor. A method for reconstructing the profile of the muon beam with the muon monitor is described in Sect. 4. In this section we also show the systematic error in the beam direction measurement, which was estimated using both the actual beam data and MC simulation. The stability of the beam direction and its intensity during T2K beam operation is discussed in Sect. 5. During the beam operation, measurements of the absolute muon yield were conducted using an emulsion detector. This result, and a comparison with the MC prediction, are shown in Sects. 6 and 7 respectively.

2. Overview of the T2K experiment

T2K consists of a neutrino beamline, producing an intense muon neutrino beam; a near detector complex, containing the INGRID on-axis detector and ND280 off-axis detector; and a far detector, Super-Kamiokande (Super-K). Using this setup, the experiment aims to measure the neutrino oscillation parameters. An overview of the T2K experiment is shown in Fig. 1. The Japan Proton Accelerator Research Complex (J-PARC) is a facility situated in Tokai, Japan. A proton beam is accelerated up to 30 GeV by the main ring synchrotron and is fast-extracted to the neutrino beamline. The neutrino beamline consists of a primary and secondary beamline, as shown at the top of Fig. 2. In the primary beamline, the proton beam is transported to a graphite target every 2 to 3 seconds. A single beam spill has a time structure of eight narrow bunches, 58 ns long with 581 ns spacing. The beam forms a two-dimensional Gaussian distribution of ∼4 mm 1 σ width corresponding to ∼7 mm radius at the target. The target and other equipment used to produce the neutrino beam is situated in the secondary beamline, the details of which are given in Sect. 2.1. The neutrino beam produced here is detected at ND280 and Super-K, and the oscillation parameters are then measured.

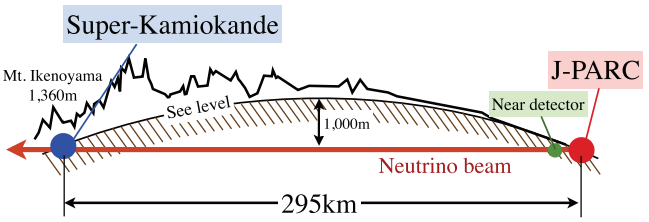

Fig. 1. Overview of the T2K experiment.

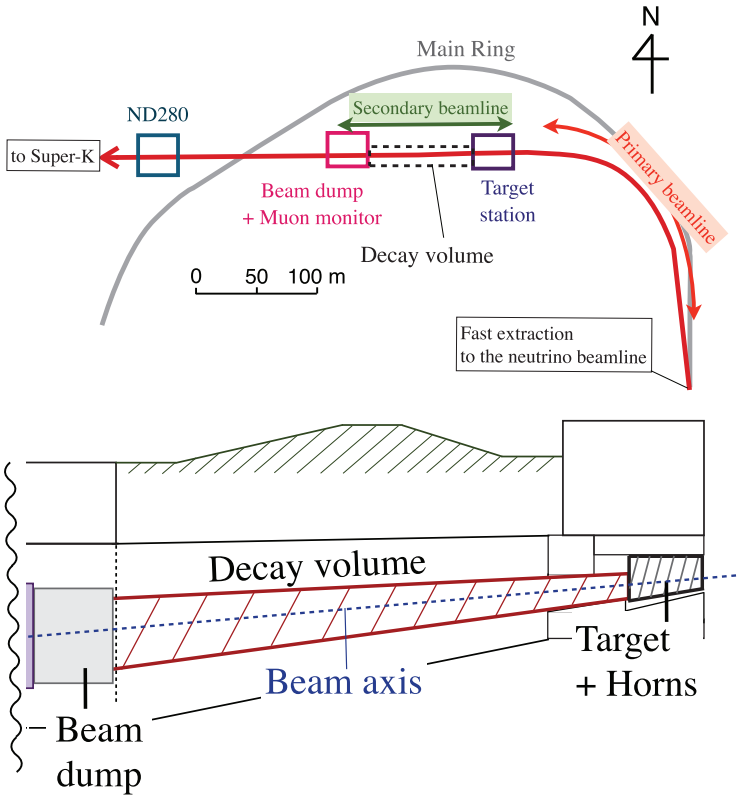

Fig. 2. Top: Overview of the T2K beamline. The beam line consists of a primary and secondary beamline. Bottom: Sideview of the secondary beamline. All of the components in the beamline, the target, horns, decay volume and beam dump, are contained in a single volume of 1500 m^3 filled with helium gas.

2.1. Creation of the neutrino beam at the secondary beamline

The bottom schematic in Fig. 2 provides an overview of the secondary beamline. All of the components in the beamline are contained in a single volume of $\sim$ 1500 m^3 filled with helium gas, which is enclosed in a helium vessel. The proton beam, transported to the target via the primary beamline, first enters a baffle which functions as a collimator. After passing through the baffle, the proton beam collides with and produces secondary particles, mostly pions. Three magnetic horns [3] are used to focus (defocus) these positively (negatively) charged pions along the designed beam-axis. Each of the horns is made of aluminum conductor and produces a maximum toroidal magnetic field of 1.7 T inside the conductor at the nominal horn current of 250 kA. The decay volume for the pions is a 96 m-long steel tunnel. A pure and intense muon neutrino beam is produced as the pions decay in this tunnel. The beam dump (see Fig. 8) sits at the end of the decay volume to absorb the hadron flux

from the beam. It consists of a core composed of 75 tons of graphite and is 3.174 m long. Fifteen (two) iron plates are placed outside (inside) the helium vessel at the downstream end of the core.

2.2. Importance of measuring the neutrino beam direction and intensity

Both ND280 and Super-K are located 2.5° from the beam-axis. This experimental setup enables us to utilize a narrow-band neutrino beam with a peak energy around 0.6 GeV at which neutrinos oscillate with near the maximum probability after traveling 295 km. However, a 1 mrad uncertainty in the beam direction measurement leads to a 2%–3% uncertainty in the neutrino energy scale, affecting measurements of the neutrino oscillation parameters. Therefore the beam direction has to be monitored with high precision and finely controlled in order to eliminate the additional uncertainty for the oscillation parameters. In addition, a contingency may arise in the beamline during operation, such as a sudden drop in the horn currents or deterioration of the target, resulting in a decrease in the neutrino beam intensity. Therefore, monitoring not only the direction but also the intensity of the neutrino beam has to be done on a spill-by-spill basis in order to promptly confirm the state and health of the beamline components as well as the quality of the neutrino beam. When issues arise in the online monitoring during beam operation, the run is immediately stopped and the status of the accelerator and beamline equipment are checked.

2.3. Beam monitors

T2K employs two beam monitors for the beam direction measurement, INGRID and the muon monitor. INGRID [4] is located 280 m downstream of the target. It has 14 independent modules which are composed of iron plates sandwiched between scintillator planes. The modules are installed at positions in a cross shape centered on the beam-axis. The profile of the neutrino beam is reconstructed by counting the number of neutrino interactions in each of the modules. Due to the small cross section of the neutrino interactions, the time for accumulating neutrino events depends on the beam intensity and typically requires one day for the profile reconstruction with a proton beam power of ∼100 kW.

The T2K muon monitor is another beam monitor that monitors the muon beam which is produced together with the neutrino beam from the decay of pions. The monitor is located 118 m downstream of the target and just downstream of the beam dump which absorbs the hadron flux. Unlike the INGRID measurement, the muon monitor can detect the muon beam spill-by-spill. Therefore, the intensity and direction of the neutrino beam can be indirectly monitored with the muon monitor on a spill-by-spill basis. It is necessary to monitor the muon beam direction with a precision of 0.3 mrad in order to control the neutrino beam direction to within 0.3 mrad with respect to the beam-axis.

3. Instrumentation of the muon monitor

The T2K muon monitor was installed 18.5 m underground in the muon pit, located just downstream of the beam dump. Details of the design of the monitor are described in [2]. The thickness of the beam dump is chosen to minimize the hadron flux while retaining a sensitivity in the measurement of the muon beam direction; only muons with energy above 5 GeV can pass through the beam dump and reach the muon monitor. Schematic diagrams of the muon monitor are shown in Fig. 3. The monitor consists of two independent detectors: an array of ionization chambers and another array of silicon PIN photodiodes. Each detector array has $7 \times 7 = 49$ sensors at 25 cm intervals and covers an area of $150 \times 150\,\mathrm{cm}^2$ with respect to the beam-axis. There is also an additional silicon PIN photodiode mounted on a small moving stage behind the silicon array (see Fig. 3) and this is used for the sensor-by-sensor calibration. This calibration is described in Sect. 4.3.

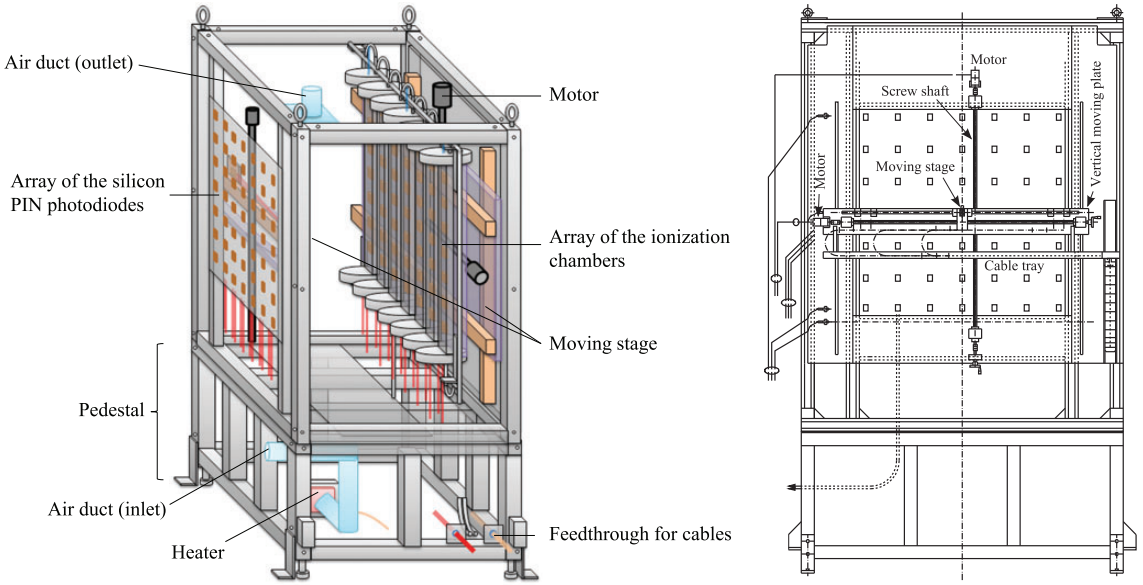

Fig. 3. Left: Schematic view of the muon monitor. The monitor consists of arrays of ionization chambers and silicon PIN photodiodes. The muon beam passes through the array of silicon PIN photodiodes first and then the ionization chambers [2]. Right: Moving stage for the calibration silicon PIN photodiode, as viewed from downstream.

3.1. Ionization chamber

Each of the seven ionization chambers contains seven sets of two parallel $100 \times 100\,\mathrm{mm}^2$ ceramic plates separated by 3 mm. One of the two parallel plates has a signal electrode which has a dimension of $75 \times 75\,\mathrm{mm}^2$ and is surrounded by the ground electrodes. A bias voltage of 200 V is applied to a $93 \times 93\,\mathrm{mm}^2$ electrode on the other plate and a uniform electric field is created through a $75 \times 75\,\mathrm{mm}^2$ area between the two electrodes. Thus, ionization pairs generated only in the $75 \times 75 \times 3\,\mathrm{mm}^3$ volume contribute to the signal. All of the chambers are filled with a gas mixture set to be 98% Ar and 2% N_2 for a beam intensity below 2.3×10^{13} protons per bunch (p.p.b.). For higher beam intensity, 99% He and 1% N_2 is used instead as the size of the signal with He gas is $\sim$10 times smaller than that with Ar gas. In both of the gas systems, N_2 is used as a quencher and to render the signal insensitive to the amount of impurities in the gas via the Jesse effect [5].

A non-linearity of the detector response is considered to be caused by a recombination of electrons and ions, resulting in depletion of the signal. We had tested the effect of the recombination at the beam test [2] and confirmed that linearity in the signal response is guaranteed up to 1.8×10^{13} p.p.b. for $Ar + N_2$ and 3.0×10^{14} p.p.b. for $He + N_2$.[1,2]

3.2. Silicon PIN photodiode

The silicon PIN photodiode (HAMAMATSU® S3590-08) has an active area of $10 \times 10\,\mathrm{mm}^2$ and a depletion layer thickness of 300 μm. The silicon layer is mounted on a ceramic base. In order to

[1] The $Ar + N_2$ gas of the ionization chamber is planned to be replaced with $He + N_2$ when the beam intensity reaches 2.3×10^{13} p.p.b. Near this beam intensity, about 5% of the deficit of the signal is expected to be observed due to the recombination of the electrons and ions. We decided this beam intensity is the limit for usage of $Ar + N_2$ gas.

[2] The expected p.p.b. is 4.8×10^{13} at 750 kW with the repetition cycle of 2.48 s.

fully deplete the layer, a bias voltage of 80 V is applied. The photodiode is attached to a PEEK^{TM} base fixed to the support enclosure and is covered by an aluminum base.

The linearity in the signal response of the silicon PIN photodiode was measured at the beam test as well as the ionization chamber, and is guaranteed up to 1.7×10^{14} p.p.b.

The silicon PIN photodiode is not tolerant of the severe radiation in the muon pit. There is a report [6] that the depletion voltage of the silicon PIN detector falls 50% at about 0.7×10^{13} protons cm^{-2} and reaches a minimum at 1.25×10^{13} protons cm^{-2}. The decrease in the signal was also reported in the beam test where a 100 MeV electron beam was used [2]. From these results, it was estimated that the signal starts to decrease after a one month exposure to the muon beam in the case of 0.75 MW beam operation.

3.3. Electronics

Both signals from the ionization chamber and silicon PIN photodiodes are transmitted by about 70 m of coaxial cables which connect the muon pit underground to an electronics hut on the surface. The signals are digitized by Flash-ADC modules (FADC) of the COPPER system [7] developed by KEK. The resolution and sampling rate of the FADC are 12 bits and 65 MHz, respectively. For the signal from the ionization chamber, the gain in the FADC is set to 5. On the other hand, unity gain is set for the signal from the photodiodes since the size of the signal is about 30 times larger than the signal from the ionization chambers. Instead, the signal from the photodiode is attenuated by 0, 15, and 30 dB, depending on the beam intensity. Both FADC and signal cable are well calibrated with a CAMAC charge/time generator (Phillips 7120) with 1% precision. A baseline shift in the electronics due to pulse pileup might affect the linearity of detector response as we use it as a pedestal for calculation of the charge (see Sect. 4.1). However, the effect of a baseline shift on the collected charge was estimated to be less than 1% for all planned beam intensities. Therefore, the effect is negligible for our analysis.

4. Measurement of the muon beam direction

The signal from each of the sensors is read out by the FADC and integrated to calculate the collected charge. The profile of the muon beam is then reconstructed by fitting the two-dimensional charge distribution with a two-dimensional Gaussian function. Details of the analysis method are described in Sect. 4.1. We also prepare a MC simulation for the prediction of the muon flux: simulation of hadronic interactions inside and outside of the target and calculation of the particle decay in the decay volume. Section 4.2 explains the simulation in more detail. The sensors are calibrated using the actual beam at the beginning of each beam operation period as described in Sect. 4.3. The systematic error for the beam direction measurement was estimated using MC simulation and beam data; this is detailed in Sect. 4.4.

4.1. Reconstruction of the muon beam profile

The collected charge is calculated for each sensor by integrating a waveform digitized by the FADC after subtracting the baseline. The typical waveforms recorded during beam operation are shown in Fig. 4. These waveforms were obtained at a beam intensity of 1.3×10^{13} p.p.b. where the attenuator level was set to 30 dB for the signal from the silicon sensors. In the analysis, the integration windows are set to each bunch and the profile of the muon beam can be reconstructed bunch-by-bunch. In this way, it is possible to measure the muon beam direction and intensity for each bunch. The single

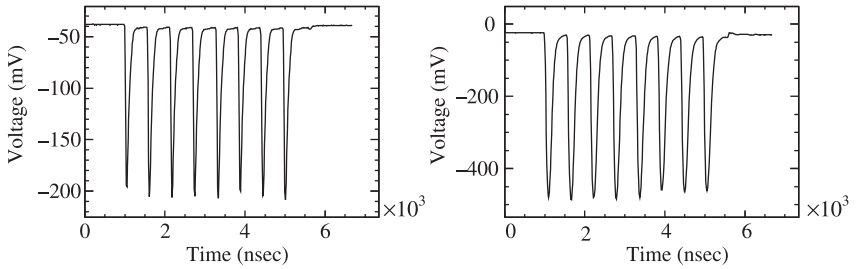

Fig. 4. Waveform of the signal from the silicon PIN photodiode (left) and ionization chamber (right), digitized by the FADC. Both of the signals are from sensors placed at the center of the arrays and recorded when the beam intensity is 1.3×10^{13} p.p.b. The attenuator level was set to 30 dB for the signal from the silicon sensors.

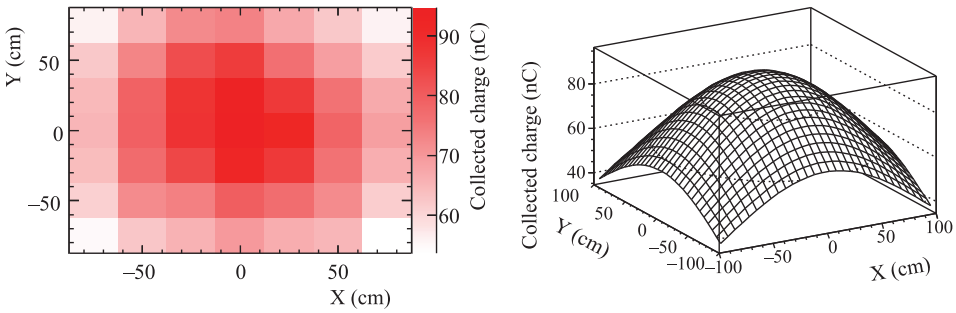

Fig. 5. Charge distribution (left) and reconstructed profile (right) of the muon beam measured by the silicon array. The collected charge is obtained for each sensor by integrating the waveform of all of the bunches (i.e. spill) read out by the FADC. This is a beam event when the intensity is 1.3×10^{13} p.p.b.

bunch measurement is affected by bunch-by-bunch fluctuation in the proton beam direction and intensity. Therefore, the muon beam direction and intensity are also reconstructed for an entire spill by summing the collected charge over all bunches in that spill. We monitor this spill-by-spill beam direction and intensity and check them for corresponding bunches when issues are found for some spills. The left panel in Fig. 5 shows the charge distribution measured by the silicon PIN photodiodes, which is obtained by summing the distribution over all bunches. In order to extract the profile of the muon beam, the distribution is then fitted by a two-dimensional Gaussian function defined as follows:

$$f(x, y) = A \exp\left[-\frac{(x - x_0)^2}{2\sigma_x^2} - \frac{(y - y_0)^2}{2\sigma_y^2}\right], \tag{1}$$

where A is a normalization parameter; x_0 and y_0 represent the centers of the beam profile in the horizontal and vertical direction, respectively; σ_x and σ_y represent the widths of the beam profile in the horizontal and vertical direction, respectively. Here the x_0 and y_0 are positions relative to the designed beam-axis at the muon monitor. In the beam direction measurement, we apply corrections for the effects of the tilted beamline and misalignment of the monitor, which are described in Sects. 4.4.2 and 5.2, respectively. An example of the reconstructed profile obtained from a fit of the two-dimensional Gaussian is shown on the right in Fig. 5. Figure 6 shows profiles of the muon beam for horn currents of 0 kA and 250 kA. The peak charge collected at 250 kA operation is about our times larger than that collected at 0 kA operation. Table 1 summarizes the center and width of the reconstructed profile for the data and MC simulation when the horns are operated at 250 kA. The muon beam direction $\{\theta_x, \theta_y\}$ is then calculated using the parameters $\{x_0, y_0\}$ and the distance $(= L)$

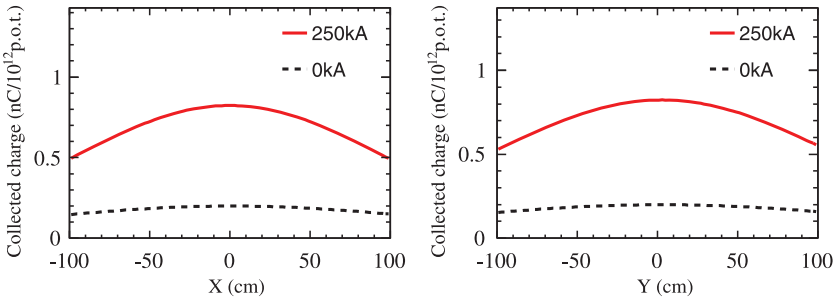

Fig. 6. Reconstructed muon beam profile obtained with the silicon array when horns are operated at 0 kA (dashed black) and 250 kA (solid red). The horizontal (vertical) profile is shown on the left (right).

Table 1. Comparison of the center and width of the beam profile between the data and MC prediction at 250 kA horn operation. In the MC simulation, the position and width of the proton beam at the baffle are compared with the data. The errors on the numbers are the MC statistical ones.

	Fitted profile center		Fitted profile width	
	x (cm)	y (cm)	wx (cm)	wy (cm)
Data	-0.1	-1.0	98.2	108.5
MC	-0.2 ± 0.3	-0.2 ± 0.3	97.7 ± 0.6	105.8 ± 0.8

between the target and muon monitor:

$$\theta_x = x_0/L, \quad \theta_y = y_0/L \quad (L = 118\,\mathrm{m}). \tag{2}$$

Here we use an approximation of $\tan\theta_{x(y)} \simeq \theta_{x(y)}$, as $\theta_{x(y)} \ll 1$.

4.2. Monte Carlo simulation

The MC simulation consists of two processes: a simulation of the hadronic interaction in the graphite target, and propagation of the secondary particles until they interact or decay. For the simulation of the hadronic interaction in the target, several simulators were tested and compared with the hadronic production data. Finally FLUKA2008 [8] was chosen, which was found to be in good agreement with the data.[3,4] Kinematic information for particles emitted from the target is saved and transferred to the JNUBEAM simulation [9]. JNUBEAM is a GEANT3 [10] simulation of the secondary beamline including the muon monitor. The geometry of these components is modeled based on the final mechanical drawings of the constructed beamline. Hadronic interactions are modeled by GCALOR [11] in JNUBEAM. Table 2 shows the MC estimation of flux of particles penetrating the muon monitor at the 250 kA horn current setting. The muons are accompanied by soft components such as gammas and δ-ray electrons. The particles contributing to the signal at the muon monitor are also estimated using the MC simulation where argon gas is used for the ionization chamber and all horn currents are set to 250 kA. The result is shown in Table 3. In both the silicon and ionization chamber arrays, the muons account for about 80% of the total signal. The subsequent contribution to the signal comes from δ-rays, accounting for about 10% of the total. A breakdown of the muon

[3] Recently FLUKA2011 was found to be the best agreement with external hadron production data.
[4] The hadron interactions are further tuned with the external experiment data in Sect. 7.

Table 2. Breakdown of the particles ($/10^{13}$ p.o.t.) arriving at the muon pit and going through the area covered by the muon monitor ($150 \times 150\,\mathrm{cm}^2$). These are estimated by the MC simulation with 250 kA horn current settings.

Particle type	Particles at the silicon array	Particles at the chamber array
μ^+	2.39×10^{10} (49.3%)	2.20×10^{10} (52.0%)
μ^-	0.18×10^{10} (3.7%)	0.17×10^{10} (3.9%)
e^-	0.32×10^{10} (6.7%)	0.26×10^{10} (6.3%)
e^+	0.03×10^{10} (0.6%)	0.02×10^{10} (0.6%)
γ	1.92×10^{10} (39.6%)	1.56×10^{10} (37.0%)
others	$<0.01 \times 10^{10}$ (0.1%)	$<0.01 \times 10^{10}$ (0.2%)
Total	4.84×10^{10} (100%)	4.22×10^{10} (100%)

Table 3. Breakdown of the particles ($/10^{13}$ p.o.t.) contributing to the signal at the muon monitor. The number listed in the table is estimated for particles going through the area covered by the monitor ($150 \times 150\,\mathrm{cm}^2$). In this MC estimation, argon gas is used for the ionization chamber and horn currents are set to 250 kA.

Particle type	Particles at the silicon array	Particles at the chamber array
μ^+	2.39×10^{10} (82.2%)	2.19×10^{10} (83.4%)
μ^-	0.18×10^{10} (6.1%)	0.17×10^{10} (6.3%)
e^-	0.30×10^{10} (10.2%)	0.25×10^{10} (9.3%)
e^+	0.03×10^{10} (0.9%)	0.02×10^{10} (0.9%)
γ and others	0.02×10^{10} (0.6%)	$<0.01 \times 10^{10}$ (<0.1%)
Total	2.90×10^{10} (100%)	2.63×10^{10} (100%)

Table 4. Breakdown of the muon flux by the parent particles ($\pi^\pm$, $K^\pm$, and K^0_L) for the 250 kA horn current setting.

Parent particle	μ^+ (μ^-)
π^+ (π^-)	91.73% (94.71%)
K^+ (K^-)	8.26% (5.13%)
K^0_L	0.01% (0.16%)

flux by the parent particles $\left(\pi^\pm, K^\pm, \text{and } K^0_L\right)$ is shown in Table 4. As listed in the table, 92% (95%) of total μ^+ (μ^-) production is attributable to parent π^+ (π^-) decays. Table 5 shows the breakdown of parent particles ($\pi^\pm$ and $K^\pm$) generated at each of the materials in the secondary beamline. Most of the pions contributing to the muon flux are generated at the graphite target. The subsequent contributions from pions come from interactions at the beam dump (carbon) which is placed just in front of the muon monitor.

Figure 7 shows p–θ phase space of the parent π^+ contributing the neutrino flux at Super-K and the muon flux at the muon monitor, where p is the momentum and θ is the polar angle with respect to the beam-axis. The phase space is estimated for the 250 kA horn setting. As seen in the figure, the majority of the parent pions for the neutrino flux at Super-K have momentum of $\sim$2 GeV/c and $\theta = 0.1$–0.2 rad. On the other hand, the muon monitor measures the muons from the forward-angle

Table 5. Breakdown of the muon parent particles generated at each material for the 250 kA horn setting. The last column shows the breakdown for the total flux. A symbol in parenthesis denotes the main material element.

Material	π^+	π^-	K^+	K^-	Total
Graphite target (C)	94.0%	64.0%	89.8%	53.9%	91.6%
Horn (Al)	1.5%	3.9%	1.2%	1.0%	1.7%
Decay volume (He)	1.2%	6.7%	1.0%	3.3%	1.6%
Decay volume (Fe)	0.4%	3.9%	0.7%	2.8%	0.6%
Beam dump (C)	2.4%	20.8%	7.2%	38.4%	4.1%
Other materials	0.5%	0.6%	0.3%	0.5%	0.5%
	100%	100%	100%	100%	100%

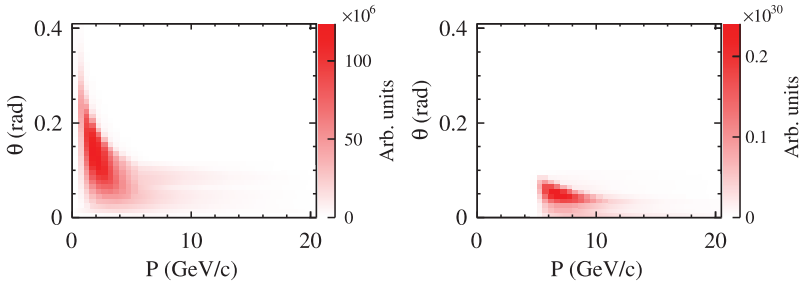

Fig. 7. p–θ phase space of the parent π^+s contributing the neutrino flux at Super-K (left) and the muon flux at the muon monitor (right), where p is the momentum and θ is the polar angle with respect to the beam-axis. These phase spaces are estimated for the 250 kA horn setting. The same p.o.t. (1.0×10^{21} p.o.t.) is used for the normalization in both the left and right plots.

pions with high momenta (>5 GeV/c). This is because only muons with energy above 5 GeV can pass through the beam dump and reach the muon monitor. Thus the phase space covered by the muon monitor has only a small overlap with that for the neutrino flux. This implies that the beam direction measured by the muon monitor might be different from that for the neutrino flux when the direction is largely shifted from the designed beam-axis. Therefore, it is highly important to keep the beam direction close to the design axis, to understand the response of the muon monitor and to confirm the neutrino beam direction by INGRID.

4.3. Detector calibration

The relative gains of the sensors are calibrated using the beam at the beginning of each beam operation period. The ionization chamber is calibrated by moving the entire chamber array by ±25 cm, which corresponds to the sensor spacing, in both the horizontal and vertical direction and measuring the muon profile at nine different configurations. These nine measured profiles should be the same on the assumption that the muon beam profile itself does not change over the course of the measurements. At each position, we have at most nine measurements of the collected charge by different sensors. The relative gains of the sensors are then estimated by comparing these charges, and the correction factors for the gain are determined so that the charges match. In order to estimate the uncertainty on the correction factors, these nine measurements, together with one more measurement at the nominal position, are subdivided into two data sets, namely five measurements for each. The correction factors are determined with each data set in the same way as above. The root mean square (RMS) of the

differences of 49 correction factors between two data sets is taken as the uncertainty of the correction factor.

The silicon PIN photodiodes are calibrated sensor-by-sensor by measuring the muon beam with an extra calibration sensor mounted on a small moving stage behind the silicon array (see Fig. 3). The calibration sensor is placed behind each sensor and the ratio of the charge collected by the calibration sensor to that of the fixed signal sensors is calculated:

$$R_i = Q_i / Q_{\mathrm{ref}} \quad (i = 1, 2, \ldots, 49), \tag{3}$$

where Q_{ref} and Q_i are the collected charges obtained by the extra calibration sensor and the ith signal sensor, respectively. The correction factor is then calculated for each sensor using the mean of the charge ratios:

$$G_i = \langle R \rangle / R_i. \tag{4}$$

This correction is then applied to each sensor. The uncertainty in the correction factor is due to the statistical error on the collected charge and it determines the precision of this calibration.

For the ionization chamber, all of the sensors are calibrated with a precision of 0.4% which is determined from the difference in the correction factors between the two data sets as described above. For the silicon PIN photodiodes, the calibration is done with a precision of 0.1% which originates from the statistical fluctuation of the measured collected charge.

4.4. Systematic error in the beam direction measurement

The systematic error in the beam direction comes from:

(1) uncertainty of the structure of the upstream materials,
(2) δ-ray contamination in the muon beam,
(3) uncertainty in the relative calibration of the sensors,
(4) alignment error of the muon monitor,
(5) effect from the tilted beamline.

The first three sources cause a distortion in the observed beam profile and lead to an uncertainty in the beam direction. The error in the alignment between the target and muon monitor causes the error in the beam direction. The beam-axis is tilted by 3.637° downward and this results in an asymmetric profile at the muon monitor. A correction factor was estimated using the MC simulation for the measurement of the vertical direction to account for this.

4.4.1. Profile distortion

The muon beam profile is reconstructed by fitting the collected charge distribution assuming it has the form of a perfect Gaussian. However, the profile can deviate from the ideal Gaussian form reflecting the geometrical shape of the upstream materials. In addition, the secondary particles, such as δ-rays, generated at the nearby materials could further distort the observed beam profile.

The beam dump consists of multiple components, as shown in Fig. 8. Any deviation of the thickness or density of these objects from their design values causes a non-uniformity of the path length of muons and may distort the muon profile. This effect was estimated with an MC simulation. In the simulation, as an extreme case study, both the density (ρ) and thickness (d) of one half (the positive side in the horizontal direction) of each dump component are adjusted up/down by their listed errors. The obtained profile centers are then compared to the nominal one. Table 6 summarizes the adjusted components of the beam dump and the resultant shifts of the profile center from the nominal values.

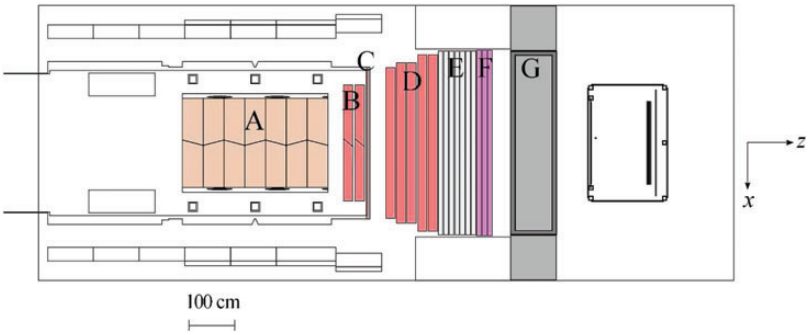

Fig. 8. Top view of the beam dump. A: graphite core. B–F: Fe plates. G: concrete wall. The beam enters from the left side.

Table 6. Density (ρ), thickness (d), and their uncertainties of the dump graphite core, Fe plates and concrete wall (see Fig. 8). The errors marked with $*$ are obtained from JIS G3193 and the tolerance listed in the document is taken as the $3\,\sigma$ error for this analysis. The other errors are from measurements. The shift of the profile center is estimated for the case ρ and d of one half of each component are adjusted by their errors.

	Material	ρ (g/cm^3)	d (cm)	Profile center shift (cm)
A	Graphite	1.707 ± 0.009	45.001 ± 0.003	Negligible
B	Fe	7.83 ± 0.03	$20.00^{+0.24}_{-0.12}$ *	0.107
C	Fe	7.85 ± 0.02 *	$8.00^{+0.17}_{-0.09}$ *	0.054
D	Fe	7.83 ± 0.03	$20.00^{+0.24}_{-0.12}$ *	0.169
E	Fe	7.8435 ± 0.0083	10.083 ± 0.033	0.083
F	Fe	7.85 ± 0.02 *	$10.00^{+0.23}_{-0.11}$ *	0.126
G	Concrete	2.30 ± 0.023	100	0.276
			Total	0.38

In total, a value of 0.38 cm (0.032 mrad) was assigned to the systematic error of the profile center (beam direction).

The other source of distortion of the profile is soft secondary particles (δ-rays and γs) from nearby materials. We have evaluated the effect of profile distortion due to the surrounding materials in two ways. The muon monitor covers an area of $150 \times 150\,\text{cm}^2$ transverse to the beam-axis while the actual profile width ($1\,\sigma$) of the muon beam is typically 100–110 cm at the monitor when the horns operate at 250 kA. Thus, the muon monitor covers ~50% of the profile region. In order to check how the actual profile deviates from the ideal Gaussian shape, the ionization chamber arrays were moved by ±25 cm to take the tail of the profile into account. Then, the fit was done for the different portions of the same profile. If the profile has a perfect Gaussian shape, the fitted result will always be same at different positions of the array. However, the result showed that there are differences in the fitted values. The maximum differences among the fitted profile centers are 1.25 cm (0.106 mrad) for the horizontal direction and 1.12 cm (0.095 mrad) for the vertical direction. During beam operation, a discrepancy of the profile center has been observed between the chamber and silicon arrays (0.55 cm in the horizontal direction and 1.77 cm in the vertical direction). This discrepancy is considered to be due to the difference of the nearby structures between the chamber and silicon arrays, causing the profile to be distorted differently at the chamber and silicon arrays. The structure most likely to cause the discrepancy is the silicon moving stage just behind the silicon array (see the right panel of Fig. 3).

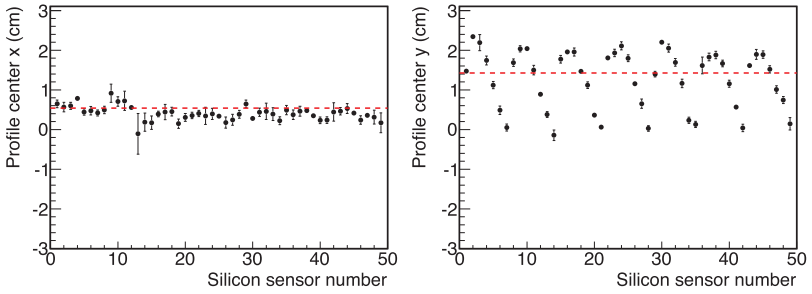

Fig. 9. Variation of the muon beam profile center measured by the chamber array during the calibration of the silicon PIN photodiodes. The dashed line shows the profile center for the same beam condition when the silicon moving stage is lowered at the bottom (nominal position).

Figure 9 shows the profile center measured by the chamber array during the calibration of the silicon array where the stage was moved to be positioned at each of the silicon sensors. When the silicon moving stage is positioned behind the top corner sensors, the profile center in the vertical direction measured by the chamber array shifts by -1.4 cm from the nominal case in which the stage is lowered to the bottom. This suggests that nearby materials affect the beam profile at the muon monitor. The shift observed in two conditions, 1.25 cm for different chamber array positions and 1.77 cm for the difference in the profile center between the silicon and chamber arrays, are taken as the systematic error. Even though part of the shift may be caused by the dump core structure, we conservatively add these errors since we cannot distinguish the effects.

As discussed in Sect. 4.3, the gains of the sensors are calibrated relatively with a precision of 0.4% for the ionization chambers and 0.1% for the silicon PIN photodiodes. The uncertainty in this calibration was propagated to the error in the beam direction. As a result, 0.08 cm (0.007 mrad) and 0.30 cm (0.026 mrad) for the horizontal and vertical directions respectively were assigned to the systematic error for the profile center (beam direction).

In conclusion, the total systematic error in the beam direction due to the profile distortion was estimated to be 2.20 cm in the horizontal direction and 2.22 cm in the vertical direction. These correspond to 0.187 mrad (horizontal) and 0.188 mrad (vertical) beam direction errors.

4.4.2. Effect of the tilted beamline against the beam dump

The beamline is tilted by 3.637° vertically while the level of the beam dump is even with the ground (see the lower half of Fig. 2). This results in asymmetric path lengths of the muons going through the beam dump with respect to the beam-axis. Thus, an asymmetric profile of the muon beam is observed at the muon monitor. This causes 1.35 cm profile center shift in the vertical direction, which was estimated using MC simulation where the center of the proton beam was set to the center of the target and parallel to the beam-axis. This shift is used for the correction in the beam direction measurement and a MC statistical error of 0.22 cm (0.019 mrad) was assigned to the systematic error of the profile center (beam direction).

4.4.3. Alignment error of the muon monitor

For the systematic error in the beam direction measurement, alignment accuracy between the muon monitor and target is also taken into account. The alignment error mainly comes from the measurement error of the relative positions of reference points between the target and muon pit, determined to be 6.1 mm for the horizontal position and 6.3 mm for the vertical position. In addition, alignment

Table 7. Summary of the systematic error for the beam direction measurement.

	Profile center		Beam direction	
Error source	Δx (cm)	Δy (cm)	$\Delta\theta_x$ (mrad)	$\Delta\theta_y$ (mrad)
Profile distortion	2.20	2.22	0.187	0.188
Tilted beam	—	0.22	—	0.019
Alignment	0.63	0.65	0.054	0.055
Total	2.3	2.3	0.19	0.20

error also comes from the setting of the muon monitor (1 mm) and the target (<1 mm). The total alignment error of the muon monitor relative to the target is therefore 6.3 mm (horizontal) and 6.5 mm (vertical). Thus, the systematic error of the muon beam direction was 0.054 mrad in the horizontal direction and 0.055 mrad in the vertical direction.

4.4.4. Summary of the systematic error on the beam direction measurement

Table 7 summarizes the systematic error for each source. Some of these systematic errors may come from the same origin, but we conservatively take the quadratic sum of these as the total systematic error. The total systematic error on the measurement of the beam direction was estimated to be 0.28 mrad ($= \sqrt{0.19^2 + 0.20^2}$). Thus, the performance of the muon monitor fulfills our requirement of 0.3 mrad.

5. Measurement of the beam direction and beam tuning with the muon monitor

Table 8 summarizes the status of T2K beam operation since the start of physics data taking in January 2010. There have been four data taking periods (RUN 1–4) in the period to May 2013. The repetition cycle (time between spills) of the proton beam has been reduced over the course of beam operations and 2.48 s was achieved for RUN 4. All three magnetic horns were operated at 250 kA during the run periods with the exception of RUN 3b where the horn currents reduced to 205 kA for most of this run. Figure 10 shows the history of the total accumulated p.o.t., as well as the beam power. The beam power has increased gradually and reached 230 kW (1.5×10^{13} p.p.b. with a 2.48 s repetition cycle) during RUN 4. The muon monitor plays an important role in measuring the direction and intensity of the muon beam, as described in Sect. 5.2. At the commissioning stage of the experiment, the horn currents were varied from 0 kA to 250 kA to check the dependence of the muon flux on the horn current. We also varied the currents by ±1% from ∼250 kA in order to check if the muon monitor is sensitive to this level of variation in the horn currents. In addition, the monitor was used as a tool for a survey of the components in the secondary beamline—this result was useful for understanding the current configuration of the baffle and target. Details of the measurement are provided in Sect. 5.5. Finally, Sect. 5.6 describes the properties of the muon and neutrino beam directions with 205 kA operation.

5.1. Proton beam tuning with the muon monitor

Figure 11 shows a schematic view of the configuration of the components in the secondary beamline, the proton-beam monitor, and the muon monitor. Before hitting the target, the proton beam passes thorough proton-beam monitors placed in the primary beamline just upstream of the secondary beamline. Segmented secondary emission profile monitors (SSEMs) are used for monitoring the profile center and width of the proton beam. The baffle is placed downstream of SSEM19 (the final SSEM

Table 8. Summary of the status of the beam operation in T2K. The second and third columns show the repetition cycle of the proton beam and the horn current, respectively. The accumulated number of p.o.t. obtained for each run is shown in the last column.

	Period	Rep. cycle (sec)	Horn curr. (kA)	Accum. p.o.t.
RUN 1	Jan 2010–Jun 2010	3.52	250	3.28×10^{19}
RUN 2	Nov 2010–Mar 2011	3.2*	250	1.12×10^{20}
RUN 3b	Mar 2012	2.92	250/205	2.15×10^{19}
RUN 3c	Apr 2012–Jun 2012	2.56	250	1.37×10^{20}
RUN 4	Oct 2012–May 2013	2.48	250	3.60×10^{20}
			Total	6.63×10^{20}

*3.04 s from March 7, 2011 to March 11, 2011.

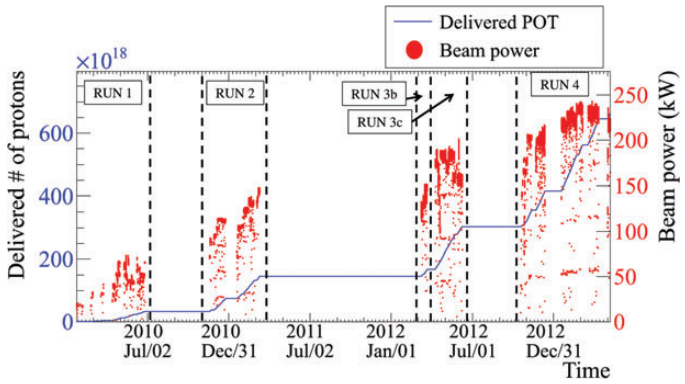

Fig. 10. History of total accumulated protons and beam power. The solid line shows the accumulated p.o.t. The dot points show the beam power.

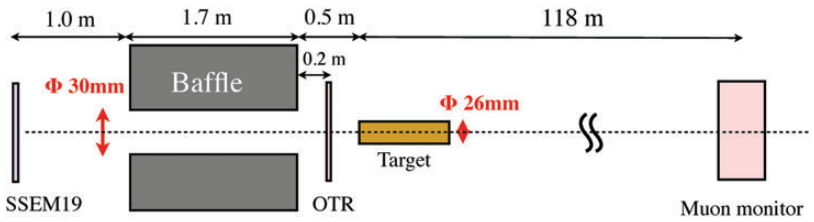

Fig. 11. Configuration of the components in the secondary beamline with SSEM19 and the muon monitor.

in the primary beamline) and plays the role of a collimator with an opening of 30 mm. An optical transition radiation (OTR) monitor [12] is placed just in front of the target and is used for the measurement of the position of the proton beam. The position of the proton beam center is extrapolated at the baffle (target) with an accuracy better than 0.7 mm (0.6 mm) from the measurements of the SSEMs and OTR. Data at various beam position were taken to measure the correlation between the proton beam position at the target and the profile center of the muon beam at the muon monitor. As shown in Fig. 12, the profile center measured by the muon monitor is very sensitive to the position of the proton beam at the target. In the figure, we also overlay the prediction by the MC simulation. In the beam tuning, the angle and position of the proton beam are tuned very precisely using this correlation such that the profile center of the muon beam is centered at the muon monitor. During

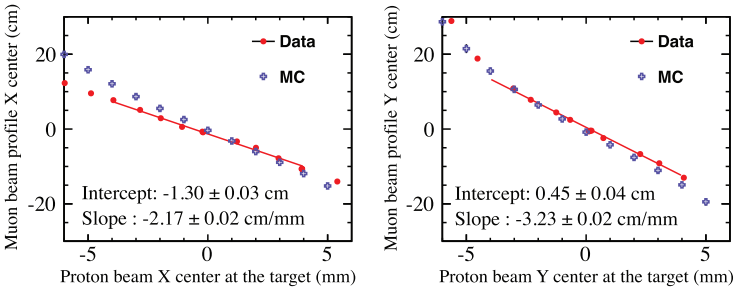

Fig. 12. Correlation between the muon beam profile center measured by the silicon sensor array and the proton beam position at the target in the horizontal (left) and vertical (right) directions. The position of the proton beam is extrapolated to the target using the measurements of the SSEMs and OTR. The red lines in the figures are results of fits to the data with linear functions in a 4 mm range around the nominal proton beam center at the target. The errors on the fitted parameters are statistical only and the MC predictions are overlaid in blue.

beam tuning the correction factor of 1.35 cm in the vertical direction, as discussed in Sect. 4.4.2, is also accounted for.[5]

5.2. Stability of the beam direction and intensity measured by the muon monitor

As described in Sect. 5.1, the proton beam is tuned using information from the muon monitor and always controlled such that the muon beam and hence the neutrino beam are positioned on the beam-axis. The stability of the response from the silicon sensors is confirmed as described below. As the radiation dose at the muon monitor sensor on the beam-axis is expected to be twice as high as that at the sensors at the edges, degradation due to the radiation damage is expected to be different depending on the sensor position in the array. The effect of different radiation doses can be estimated using calibration data taken in different periods, where signals from the sensors are measured at various positions (see Sect. 4.3). The difference in the signal size between the edge and center sensors was checked for different calibration data sets. We then checked if there was any significant decrease in the signal size at the center sensor where the radiation dose is highest. As a result, it was confirmed that there was no significant decrease in the signal size after accumulating $\sim 1.0 \times 10^{20}$ p.o.t. We therefore conclude that the response of the sensor is stable for operation accumulating $\sim 1.0 \times 10^{20}$ p.o.t., which is a typical value of p.o.t. obtained in each run period (RUN 1–3). For RUN 4 operation, where more than 1.0×10^{20} p.o.t. was accumulated, we rely on the result from the beam test and assumption discussed in Sect. 3.2. Figure 13 shows the daily stability of the muon beam as measured by the muon monitor. Figure 13(A) shows the stability of the measured total collected charge, obtained by summing up the collected charge over all the sensors, for the silicon and chamber arrays. The ratio of the total charge collected by the silicon array to that collected by the chamber array is also shown in Fig. 13(B). The large ratio observed at the beginning of RUN 4 is due to the fact that He gas was mistakenly allowed to flow into the chambers where it mixed with the Ar gas. Before the start of RUN 4 operation, all of the silicon PIN photodiodes were replaced with new ones. At the beginning of RUN 4, it was observed that their signal sizes gradually decreased and then stabilized. This also affects the stability of the ratio of the total collected charge around the beginning of RUN 4 operation and is currently under investigation. The profile center measured by the silicon and chamber

[5] As discussed in Sect. 5.2, the sensor position was mistakenly misaligned by 2.5 cm in the vertical direction, and this is also taken into account in the beam tuning.

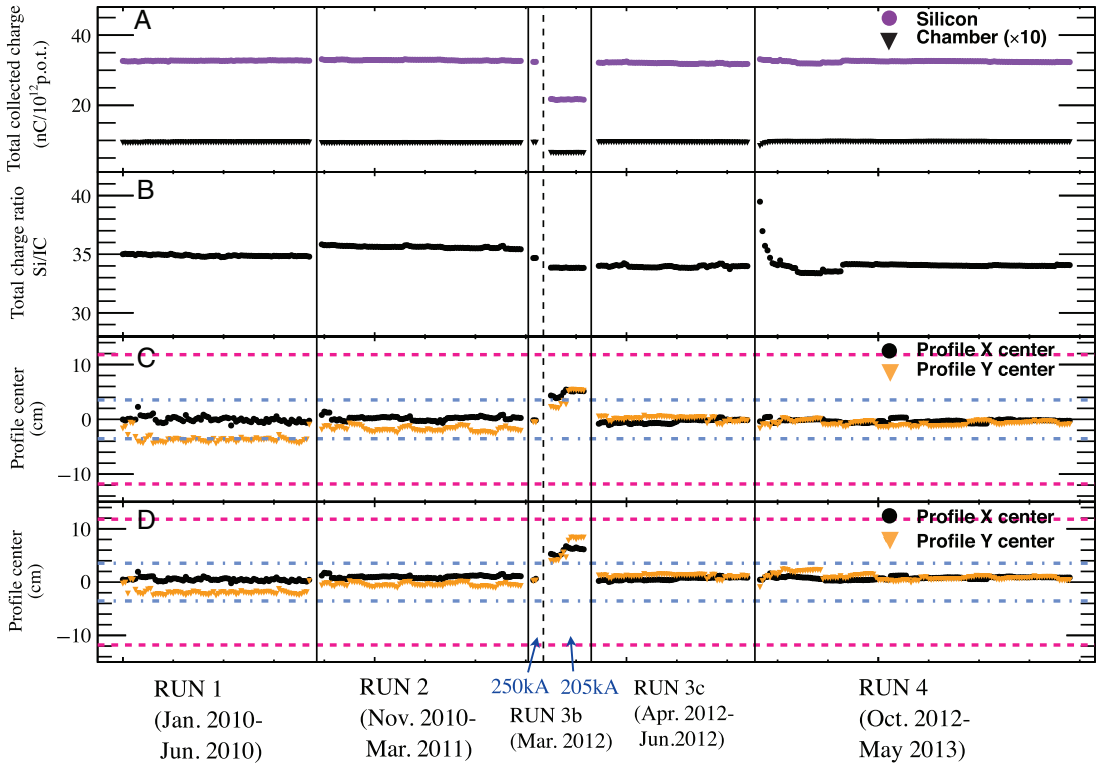

Fig. 13. Daily stability of the muon beam measured by the muon monitor. (A): The total collected charges measured by the silicon and chamber (scaled up by a factor of 10) arrays. (B): The ratio of the total charge collected by the silicon array to that collected by the ionization chamber array. (C): The profile center measured by the silicon array. (D): The profile center measured by the ionization chamber array. In plots (C) and (D), the pink and blue lines correspond to the 1.0 mrad and 0.3 mrad shifts of the beam direction, respectively.

arrays is shown in Fig. 13(C) and (D), respectively. As shown in the history of the beam direction measurement, most of the events lie within 0.3 mrad except for events that occurred during RUN 1 and RUN 3b. After RUN 1, the center position of the muon monitor was found to be mistakenly misaligned by −2.5 cm in the vertical direction. This misalignment was taken into account for the beam tuning from RUN 2 onwards. Throughout most of RUN 3b the magnetic horns operated at 205 kA, and during this time the profile center of the muon beam was shifted even though the proton beam was tuned to the center at the target using the correlation shown in Fig. 12. The direction and intensity of the neutrino beam have also been measured by INGRID and this result is shown in Fig. 14, with the neutrino event rate having been stable over the majority of the run period. The middle and bottom plots in the figure show the stability of the neutrino and muon beam direction measured by INGRID and the muon monitor respectively. As seen in the figure, there is a clear correlation in the vertical beam direction measurement between INGRID and the muon monitor over RUN 1 and RUN 2. As described above, the misalignment of 2.5 cm of the muon monitor was not taken into account in the beam tuning during RUN 1. After tuning the proton beam with this correction, both of the measurements then give vertical position close to 0 from RUN 2. On the other hand, the beam direction measured by INGRID shows a different tendency from that of the muon monitor during the RUN 3b operation. However, all of the spills were within 1.0 mrad for both the muon and neutrino beams. In addition, most of the spills were controlled well within our 0.3 mrad requirement. Table 9 summarizes the average and RMS of the profile center and total collected charge. A larger RMS of

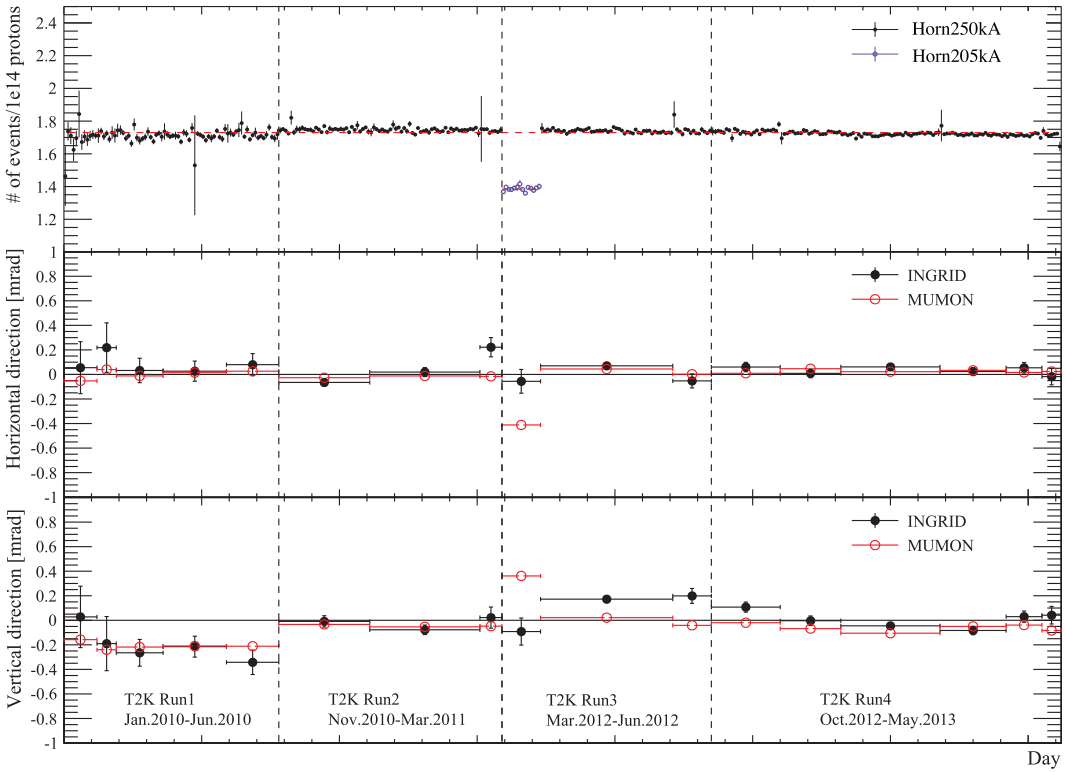

Fig. 14. Top panel shows the neutrino event rate per 10^{14} p.o.t. measured by INGRID (points) along with the mean value (dashed line); the middle and bottom panels show the beam direction measured by the muon monitor (red open circle) and INGRID (black circle) in the horizontal and vertical direction respectively. The error bars represent the statistical error only.

Table 9. Average beam profile center and total collected charge as measured by the muon monitor for each T2K run period. The numbers in parentheses denote the RMS of the spill-by-spill fluctuation. The total collected charge is calculated by summing up the collected charge over all the sensors.

	Silicon array			Ionization chamber array		
	Profile center		Total collected charge	Profile center		Total collected charge
Period	X (cm)	Y (cm)	(nC/10^{12} p.o.t.)	X (cm)	Y (cm)	(nC/10^{12} p.o.t.)
RUN 1	−0.1 (0.62)	−3.8 (0.53)	32.7 (0.7%)	0.4 (0.47)	−2.0 (0.47)	0.939 (0.7%)
RUN 2	0.2 (0.42)	−1.9 (0.48)	32.8 (0.8%)	1.0 (0.45)	−0.5 (0.46)	0.922 (0.7%)
RUN 3b (250 kA)	−0.2 (0.19)	−0.6 (0.19)	32.4 (0.5%)	0.5 (3.06)	0.2 (2.01)	0.934 (1.6%)
RUN 3b (205 kA)	4.8 (0.60)	4.2 (1.52)	21.7 (0.7%)	5.9 (1.11)	6.7 (2.18)	0.640 (0.7%)
RUN 3c	−0.4 (0.38)	0.1 (0.41)	32.0 (0.7%)	0.6 (0.44)	1.1 (0.46)	0.942 (0.6%)
RUN 4	−0.3 (0.33)	−0.8 (0.47)	32.4 (0.8%)	0.8 (0.34)	0.9 (0.66)	0.954 (1.0%)

the beam direction measurement by the chamber array was observed in RUN 3b when the horn currents were set to 250 kA at the beginning of the operation. At that time, we had gradually increased the proton beam intensity from a very low value (4.0×10^{11} p.p.b.). As a result, we were not able to obtain a good signal-to-noise ratio in the measurement of the chamber for the 250 kA operation in RUN 3b. However, this is still within the requirement and we achieved good stability in the beam

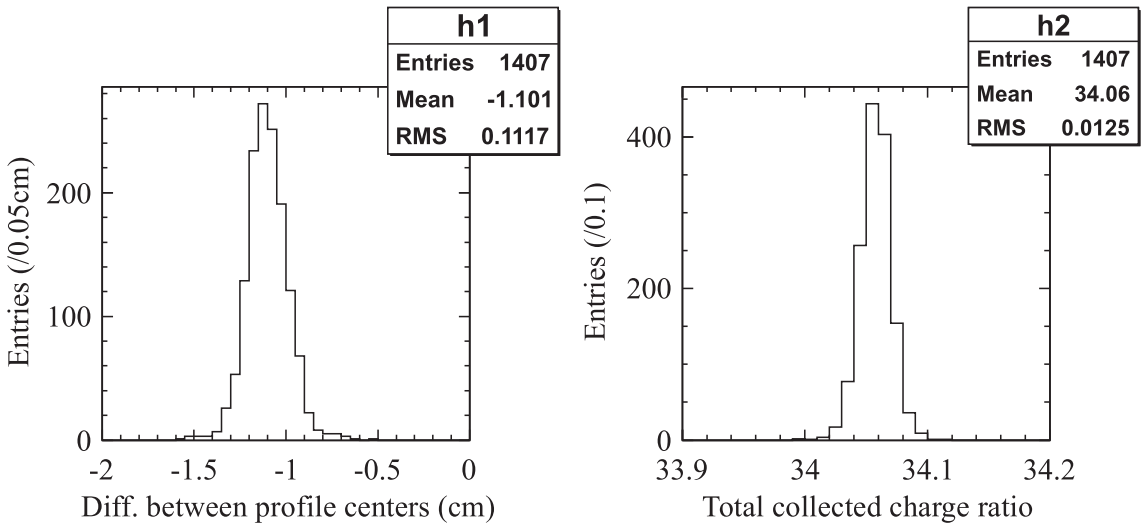

Fig. 15. Resolution of spill-by-spill measurements for the direction (left) and intensity (right) of the muon beam. For the beam direction, the differences in the measured profile center between the silicon and chamber arrays are plotted. For the beam intensity, we took the ratio of the total collected charge measured by the silicon array to that measured by the chamber array. These results were obtained with a proton beam intensity of 1.3×10^{13} p.p.b. over a 1 hour period.

direction over the entire period. The total collected charge was also kept stable with the RMS less than 1.0% for most of the span of beam operation.

5.3. Resolutions of spill-by-spill measurements for the direction and intensity of the muon beam

The direction and intensity of the muon beam can vary spill-by-spill due to the fluctuations in the proton beam direction and in the horn current. The resolution of the variation in the direction and intensity measurement by the muon monitor was estimated by comparing measurements by two independent detectors, i.e. the silicon and chamber arrays, in order to reduce the effects from intrinsic beam fluctuations. The measurement was done for a short period ($\sim$1 hour) in which beam conditions were stable. For the beam direction, we took the difference in the measured profile center between the silicon and chamber arrays as shown on the left in Fig. 15. The mean of the differences is not zero. This is considered to be due to the nearby structures between the chamber and silicon arrays, as discussed in Sect. 4.4.1. For the beam intensity, we took a ratio of the total collected charge measured by the silicon array to that measured by the chamber array (see the right panel in Fig. 15). The resolution obtained in this way is actually a (quadratic) sum of those from the ionization chamber and silicon sensors. As the size of a signal from the silicon array is 30 times larger than a signal from the ionization chambers, the resolution at lower intensity is limited by the resolution of the ionization chambers. The resolutions become better as the proton beam intensity increases. As a result, we achieve good resolutions of $<$3.0 mm for the direction and $<$0.1% for the intensity measurement when the beam intensity is above $\sim 0.5 \times 10^{13}$ p.p.b.

5.4. Dependence of the muon yield on the horn current

Increasing the horn currents results in focusing more charged pions and producing more intense muon and neutrino beams. The focusing of pions can be confirmed by the intensity of the muon beam at the muon monitor, which is measured as the collected charge in the muon monitor. During

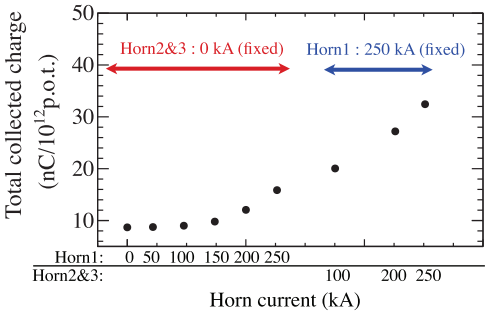

Fig. 16. Dependence of the total collected charge for different combinations of horn currents.

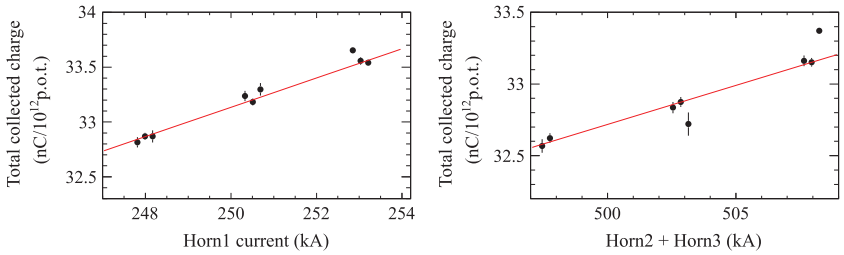

Fig. 17. Dependence of the total collected charge on the horn current variation. Left: the Horn1 current was changed by ±1% (2.5 kA) from the nominal value (250 kA) while fixing the Horn2 and Horn3 currents at 252 kA. Right: the Horn2 and Horn3 currents were simultaneously changed by ±1% (2.5 kA) from the nominal values while fixing the Horn1 current at 248 kA.

beam operation, we tested how the collected charge changes by varying the horn currents from 0 kA through to 250 kA. Figure 16 shows the total collected charge measured by the silicon array for various horn currents. When all of the horns are operated at 250 kA, the collected charge increases by a factor of four compared with the case of 0 kA horn current setting. We also varied the horn current within ±1% (2.5 kA) and checked the effect on the collected charge. This result is shown in Fig. 17. When the Horn1 current was varied by ±1 kA from 250 kA while fixing the Horn2 and Horn3 currents at 252 kA, the collected charge measured by the silicon array varied by 0.40% (left panel in Fig. 17). Subsequently, the Horn2 and Horn3 currents were simultaneously varied by ±1% from ∼250 kA while fixing the Horn1 current at 248 kA. This resulted in a 0.33% kA^{-1} change in the collected charge (right panel in Fig. 17). As described in Sect. 5.3, the muon monitor has a resolution of 0.1% in the beam intensity measurement. Thus, the monitor is sensitive to variations of ∼0.3 kA in either Horn1, or Horn2 and Horn3 combined. These results show that the muon monitor is also useful for monitoring the horn currents.

5.5. Survey of the secondary beamline

The configuration of the components in the beamline might be changing due to the sinking of the ground. In addition, the Great East Japan Earthquake in 2011 resulted in movement of many of the components [9]. The muon monitor has also played an important role in confirming the alignment of the secondary beamline. Ideally the relative center positions should be consistent between the baffle and target. If there is a difference in the relative center positions between these two components, the proton beam will hit the baffle (collimator) and will not produce secondary particles in the target effectively. In addition, the mis-steered beam, which is not collimated properly by the baffle, could

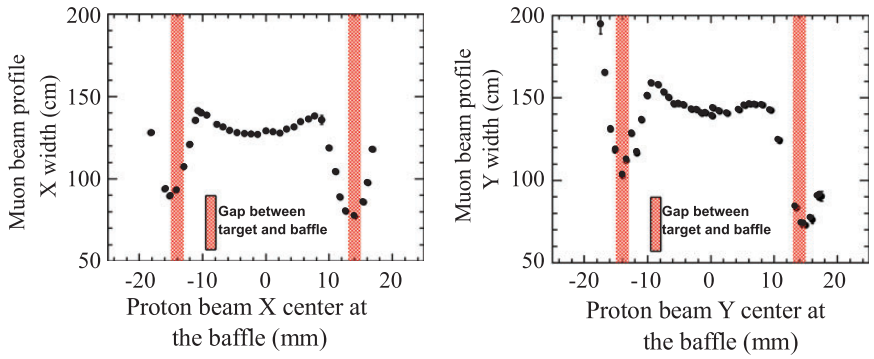

Fig. 18. Profile width of the muon beam at the silicon array obtained by scanning the proton beam at the baffle in the horizontal (left) and vertical (right) axes. The expected position of the 2 mm gap between the baffle and target is indicated as the red shaded region ($-15 \sim -13$ mm and $13 \sim 15$ mm). All of the horn currents were set to 0 kA while taking this data.

Table 10. Fitted gap position between the baffle and target. The error is statistical.

	Scan in horizontal		Scan in vertical	
	$x < 0$	$x > 0$	$y < 0$	$y > 0$
Fit result (mm)	-15.0 ± 0.04	13.7 ± 0.04	-14.1 ± 0.03	14.9 ± 0.11
Fit range (mm)	$-17.0 \sim -13.0$	$11.5 \sim 15.5$	$-16.0 \sim -13.0$	$13.0 \sim 16.5$

result in hitting downstream components. However, it is impossible to survey the instruments with a visual inspection during beam operation because they are inside the helium gas volume enclosed by the helium vessel. We therefore conducted the survey using the proton beam during operation just after the recovery work for the earthquake. The proton beam size was set to 2.3–2.8 mm during the survey run while the nominal size is ∼4 mm. As shown in Fig. 11, the baffle has a beam hole of 30 mm, while the target has a diameter of 26 mm. Thus there is a radial gap of 2 mm between baffle and target. If the alignments of these two instruments are perfect, the proton beam interacts less with the target when passing through the gap. Then the contribution of the muons from interactions at the dump increases. This results in a narrower muon beam at the muon monitor. Figure 18 shows the profile width of the muon beam at the silicon array, obtained by scanning the proton beam position at the baffle in horizontal (left) and vertical (right) axes. The expected position of the 2 mm gap between the baffle and target is expressed as the red shaded region ($-15 \sim -13$ mm and $13 \sim 15$ mm) in the figure. As shown in Fig. 18, the profile widths have minimums around the gap in both horizontal and vertical axes. Fitting to these dips with a quadratic function was performed to extract the actual gap position. The result is shown in Table 10. The fitted dips are situated within the expected position of the 2 mm gap between the baffle and target.

5.6. Properties of the muon and neutrino beam directions with 205 kA operation

In this section, we discuss the properties of the muon and neutrino beam directions when all the horns are operated at 205 kA.

In order to understand the properties of the muon beam direction during 205 kA operation, we scanned the proton beam at the target and compared the result with that obtained during 250 kA

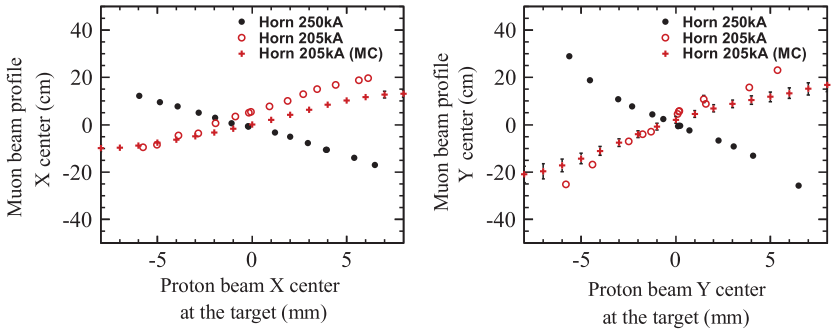

Fig. 19. Correlation between the profile center at the silicon array and the proton beam position at the target for the 250 kA (black) and 205 kA (red) operation. The MC prediction for the 205 kA horn current setting is overlaid in the same figure.

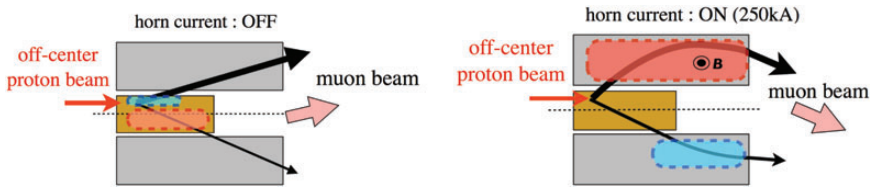

Fig. 20. Explanation of the changes in direction of the muon beam when the horn current is turned off (left) and on at 250 kA (right).

operation. Figure 19 shows the correlation between the profile center at the silicon array and the proton beam position at the target. The MC prediction for the 205 kA horn current setting is overlaid in the figure. As seen in the figure, the correlation is negative for 250 kA operation, whereas it becomes positive for 205 kA operation for both the data and MC. The reason is considered as follows. An off-center proton beam produces secondary particles asymmetrically with respect to the beam-axis because of different path lengths through the target. In the case of a 0 kA horn current setting, particles in the opposite direction of the off-center beam are more attenuated in the target (see the left panel in Fig. 20). The muon beam would then be directed in the same direction as the off-center beam, resulting in positive correlation. On the other hand, when the horn currents are turned on and the focusing becomes stronger, this results in negative correlation between the profile center at the muon monitor and the proton beam position at the target. This is considered as follows. When the proton beam is off-center at the target, differences arise in the exit points from the target between secondary particles. For example, if the proton beam hits the target in the positive direction, the secondary particles generated exit in the positive direction from the target faster than those generated in the negative direction. Those which exit the target faster experience a larger Lorentz force and are therefore more focused (see the right panel in Fig. 20). Thus, the muon beam would be directed in the opposite, i.e. negative, direction. The MC simulation was used to confirm the dependence of the profile center position of the muon beam on the proton beam position at the target with different horn currents. The result shows that correlation is lost for some horn current value between 205 kA and 250 kA. This means that the profile center of the muon beam is no longer sensitive to the proton beam position at the target for some horn current values between 205 kA and 250 kA.

The response of the neutrino beam may be different from that of the muon beam. Figure 21 shows the correlation between the profile center of the neutrino beam and the proton beam position estimated with the MC simulation. Here the profile center of the neutrino beam is simulated at 280 m

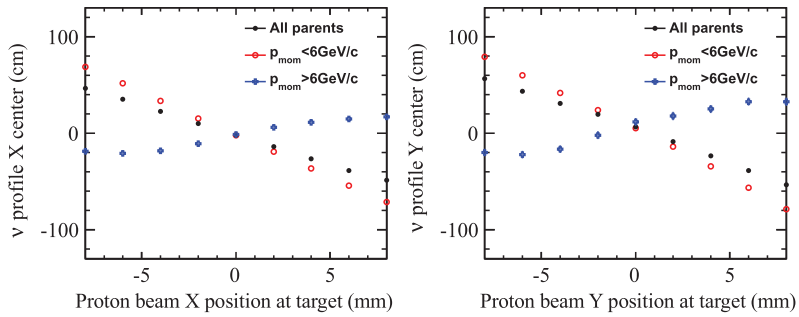

Fig. 21. Predicted correlation between the profile center of the neutrino beam at 280 m downstream of the target and the proton beam position at the target for the 205 kA horn current setting. The MC samples are categorized according to the neutrino's parent particle momentum: $p_{\mathrm{mom}} > 6\,\mathrm{GeV}$ (blue), $p_{\mathrm{mom}} < 6\,\mathrm{GeV}$ (red), and the whole momentum region (black).

downstream of the target, which is the same location at which INGRID was installed, and is categorized according to the momentum of the parent particle (p_{mom}): $p_{\mathrm{mom}} < 6\,\mathrm{GeV/c}$, $p_{\mathrm{mom}} > 6\,\mathrm{GeV/c}$, and the whole momentum region. The phase space with $p_{\mathrm{mom}} > 6\,\mathrm{GeV/c}$ is approximately the same as that covered by the muon monitor (see the right panel in Fig. 7). As seen in Fig. 21, the correlation is positive for neutrinos from the parent particles with $p_{\mathrm{mom}} > 6\,\mathrm{GeV/c}$ while it becomes negative for those from the lower-momentum parent particles ($p_{\mathrm{mom}} < 6\,\mathrm{GeV/c}$) and the overall parent particles. This indicates that the horn current of 205 kA is strong enough to focus the secondary particles with low momenta toward the opposite direction to that of the proton beam. Since the majority of neutrinos come from low-momentum parent particles, the correlation for neutrinos from the overall parent particles is also negative. This means that the response to the proton beam position at the target is different between the muon monitor and INGRID when the horns are operated at 205 kA. Therefore, it is important to keep the muon beam direction to the designed beamline axis.

6. Absolute muon yield measurement by emulsion detector

The particles arriving at the muon monitor are expected to be a mixture of muons and some lower-energy components, namely electrons and gammas as shown in Table 2. Since the standard detectors of the muon monitor, the silicon detectors and the ionization chambers, are designed to obtain the profile of the muon beam by measuring the integrated ionization in their active volumes, the measured profile is a convolution of all the components in Table 2. In fact, understanding the absolute muon flux is important for understanding the detector response of the muon monitor to various beam conditions and, therefore, the validity of its use for proton beam control. In order to complement the muon monitor measurement and to diagnose the absolute muon flux, a set of emulsion detectors was temporarily inserted during the period of commissioning.

The emulsion detector has a high spatial resolution, down to tens of nanometers, allowing a five-dimensional reconstruction of particle trajectories: three positions (X, Z, Y) and two angles ($\tan\theta_x$, $\tan\theta_y$), for particle densities of up to 10^6 particles cm^{-2}. Furthermore, by employing a proper detector structure, it can successfully reject the low-energy components by their multiple Coulomb scattering inside the detector materials.

The emulsion film used for this measurement is the recent standard emulsion film, so-called OPERA film [13], which has two sensitive 44 μm emulsion layers on both sides of a plastic base (205 μm thick) and the thickness of the film in terms of radiation length is 0.003 X_0. In order to reduce the background tracks accumulated in the emulsion film, a *refreshing* treatment [13] was previously

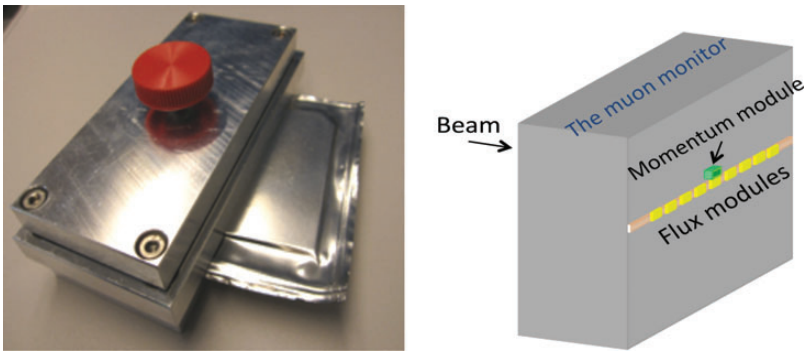

Fig. 22. Left: The flux module with eight emulsion films vacuum-packed in an aluminum laminated film and a mechanical support to maintain high flatness. Right: Schematic of emulsion detector setup.

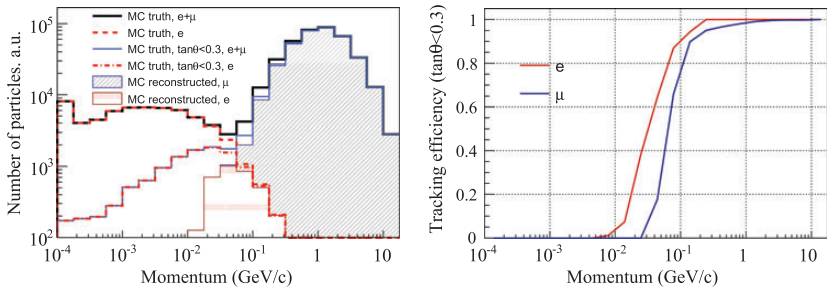

Fig. 23. Left: Momentum distribution of the input fluxes and the reconstructed particles. Right: Tracking efficiency for the particles in the angular acceptance of $\tan\theta < 0.3$.

applied. All films were placed in a climate chamber and remained at T = 28°C with R.H. = 98% for 6 days, and then dried at T = 20°C with R.H. = 50% for 1 day. An emulsion detector module (see the left panel in Fig. 22) consists of eight 6 cm × 5 cm films. A horizontal array of seven modules (separated by 25 cm) centered on the neutrino beam-axis just downstream of the muon monitor ionization chambers measures the absolute muon yield, as shown on the right in Fig. 22.

In addition to the above detector array, another detector dedicated to measuring the momentum distribution of the muons was also placed at the center of the neutrino beam. These muon momentum measurements will be the subject of a future publication.

The data readout of the emulsion films is performed with OPERA scanning microscopes [14] and the tracks crossing several films are reconstructed by the FEDRA emulsion data analysis framework [15].

The performance of the detector module for the flux measurement is also checked with a Geant4-based MC simulation (G4). The flux input, described in Sect. 7, is propagated through the detector by G4 with the detection efficiency described later.

The energy distributions of the input fluxes and the reconstructed particles are shown in Fig. 23 on the left, as a stacked histogram with black and dashed red lines, respectively. An application of the angular acceptance of $\tan\theta < 0.3$ (where θ is the angle from the normal vector of the film surface) can effectively reduce the low-energy components because the track angles of low-energy components have less correlation with the beam angle (blue and fine dashed red lines). The reconstructed tracks which have at least four hits out of eight films, with the most upstream hit existing among the first four films, are selected for the flux measurement, and shown as a filled stacked histogram; the additional reduction of low-energy components is achieved via their multiple Coulomb scattering in

Table 11. Horn current, the number of spills, and p.o.t. for each exposure time. A systematic error of 2.6% is assigned to the p.o.t. measurement, which is determined from the calibration accuracy of the beam monitor and uncertainty in the analysis technique.

Exposure	Horn current	# of spills	($\times 10^{11}$) p.o.t.
A	250 kA	1	1.95 ± 0.05
B	0 kA	2	$1.98 + 1.95 = 3.93 \pm 0.10$

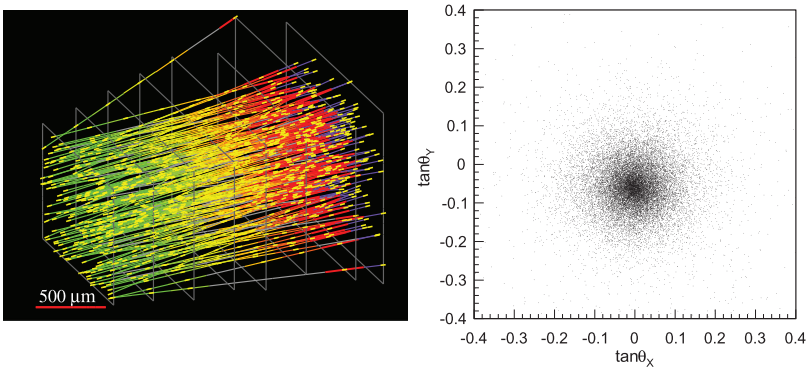

Fig. 24. Left: Example of reconstructed tracks entering a $1 \times 1\,\mathrm{mm}^2$ surface in the center module when the horn is operated at 250 kA. The color of lines shows the depth in the module. Right: The measured angular distribution in the same detector. Each dot corresponds to the individual track angle.

the eight films by requesting a stringent angular matching between the films. The track reconstruction efficiencies for muons and electrons are given in Fig. 23 on the right, as a function of their momenta. The overall detection efficiency for muons is estimated to be 98.0% with respect to the muons in the angular acceptance or 94.2% for muons in all angular space. The contamination by electrons is expected to be as small as 1.0% with respect to the number of muons reconstructed in the angular acceptance, which is estimated from the MC simulation.

The emulsion detectors were exposed to a low intensity beam twice with the different horn current settings, see Table 11. In the table, we assign 2.6% error on the p.o.t. measurement, which is determined from the calibration accuracy of the beam monitor and uncertainty in the analysis technique. The films were then photo-developed.

For each film, the data is taken from a $2\,\mathrm{cm}^2$ area at the center of the film. The relative alignments between the films are found by using the beam tracks themselves with sub-micron precision. After the track reconstruction, an effective area of $1\,\mathrm{cm}^2$ at the center of film is used to compute the flux and an angular acceptance ($\tan\theta < 0.3$) is applied. An example of the reconstructed tracks is shown in Fig. 24 on the left, with the angular distribution on the right.

The detection efficiencies of each film and module are measured using the reconstructed tracks in the module, counting the number of missing hits in the film for the tracks crossing the film, these are shown in Fig. 25. The tracking efficiency of each module is then computed by taking account of the efficiencies of individual films in the module and the track selection criteria with the angular acceptance. Since a track can be reconstructed if it has at least four hits out of eight films, the tracking efficiency is higher than the single film efficiencies. The tracking efficiencies for high-energy particles, where multiple Coulomb scattering does not contribute towards the inefficiency, are calculated to be higher than 99.5% for all modules. The flux data is corrected by the tracking efficiency module-by-module and used in later analysis.

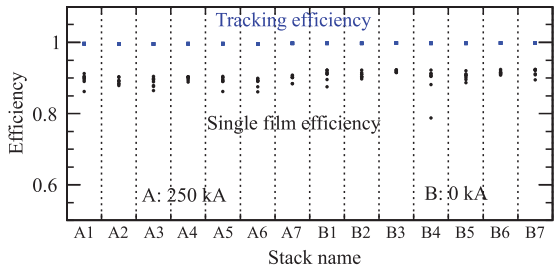

Fig. 25. Single film and tracking efficiencies for all films and modules. The efficiency is computed using all tracks with the angular acceptance of $\tan\theta < 0.3$.

The uncertainty in the flux measurement apart from the p.o.t. uncertainty was estimated by comparing measurements by two modules stacked together along the beam-axis. The difference in the number of tracks between these two modules was measured to be 2.2%, where 0.8% is expected to be due to the ionization stop at the upstream module. Therefore, the maximum observed difference is 1.4%, which might come from individual differences in the modules. Since an expected statistical fluctuation for the difference is 0.7%, we conservatively take 2% as the systematic error on the flux measurement.

The flux data is then fitted with a Gaussian function (see Fig. 28) and the muon fluxes at the profile center are obtained as $(1.09 \pm 0.01 \pm 0.03) \times 10^4$ tracks/cm^2/4×10^{11} p.o.t. when the horns are not operated and $(4.06 \pm 0.05 \pm 0.10) \times 10^4$ tracks/cm^2/4×10^{11} p.o.t. when the horns are operated at 250 kA. Here the first error denotes the error in the flux measurement due to the statistical error and the systematic uncertainty for each module. The second comes from the systematic uncertainty in the p.o.t. measurement (2.6%). The 1 σ widths of the flux profiles are measured to be 122.4 ± 6.5 cm and 105.6 ± 4.1 cm, respectively.

7. Comparison of the muon yield with prediction based on tuned simulation

As described in Sect. 4.2, T2K uses FLUKA2008 for the simulation of the hadronic interaction in the graphite target and the kinematic information for the particles is then transferred to the JNUBEAM simulation. Hadronic interactions in the JNUBEAM simulation are treated with GCALOR. For a precise prediction of the neutrino and muon flux, T2K corrects the model based on hadron interaction data provided by external experiments, primarily relying on the NA61/SHINE measurements [16]. A flow diagram for the precise estimation of the muon flux is shown in Fig. 26. This section first describes how the muon flux is predicted in Sect. 7.1. Systematic errors of the prediction are summarized in Sect. 7.2. The result is then compared with the measurement from the emulsion data in Sect. 7.3.

7.1. Correction of the muon flux

In order to make a prediction based on the external hadron interaction data, we use the method developed for the T2K flux prediction [9]. Here, we briefly summarize the procedure. The following quantities modeled in FLUKA2008 and GCALOR are corrected based on the external data:

(1) interaction rates for p, $\pi^{\pm}$, and $K^{\pm}$, and
(2) differential production of $\pi^{\pm}$, $K^{\pm}$, and K^0_L in the interaction of protons on the target.

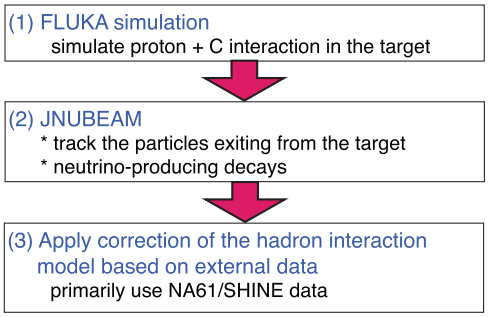

Fig. 26. Flow diagram of the flux prediction.

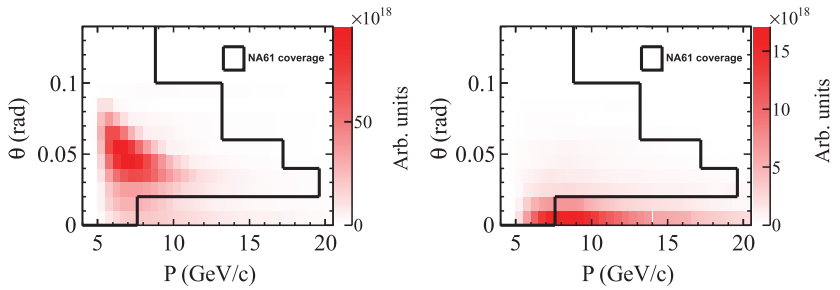

Fig. 27. Phase space of the parent π^+s contributing muon flux at the muon monitor when the horn currents are operated at 250 kA (left) and 0 kA (right). The same p.o.t. ($= 4.0 \times 10^{11}$ p.o.t.) is used for the normalization in both the left and right plots. The NA61 coverages shown in these figures correspond to the 2007 data.

The NA61/SHINE measurement provides both the differential production and the interaction rate [17,18], which are primarily used for the prediction of the neutrino and muon flux. Other experimental data are used to compensate for the measurement of NA61/SHINE [19–21].

The hadronic interaction rate is given by a so-called production cross section (σ_{prod}) which is calculated by subtracting the cross section for the quasi-elastic scattering process (σ_{qe}) from the total inelastic cross section (σ_{inel}):

$$\sigma_{\text{prod}} = \sigma_{\text{inel}} - \sigma_{\text{qe}}. \tag{5}$$

Most of the data provides σ_{inel}. In order to extract σ_{prod}, σ_{qe} is estimated from hadron + nucleon scattering data using a method based on [22] and is subtracted from σ_{inel}. The production cross section is also estimated from both FLUKA2008 and GCALOR and is compared to the data. The prediction of FLUKA2008 was found to be in good agreement with the data. Therefore, the correction of σ_{prod} using the data is applied only for GCALOR.

Figure 27 shows the phase space of the parent π^+ contributing to the muon flux at the muon monitor when the horn currents are set at 250 kA (left) and 0 kA (right). Most of the phase space is covered by the NA61/SHINE data for the 250 kA operation. On the other hand, only π^+s in the forward angle regions reach the muon monitor for the 0 kA operation. This results in only approximately 30% coverage by the NA61/SHINE data. Most of the K^+s contributing to the muon flux are not covered by the NA61/SHINE data.[6] The differential production depends on the incident particle momentum, p_{in}, and target nucleus, A. For secondary $\pi^\pm$s produced by 31 GeV/c protons in the

[6] The correction of the flux was performed using results from the NA61/SHINE measurement in 2007. NA61/SHINE also collected data in 2009, where statistics increased by an order of magnitude as compared

phase space covered by NA61/SHINE data, corrections are directly applied using the NA61/SHINE data. The corrections for tertiary pion production from secondary particles and for the production at materials (A) other than graphite are obtained with extrapolations from the NA61/SHINE data assuming momentum and A-dependent scaling [23–26].

The correction for the production of K^+ and K^- in the phase space not covered by the NA61/SHINE data is estimated with other experimental data [19,20]. For the hadrons in phase space uncovered by any experimental data, the corrections are no longer applied.

As a result of the correction the absolute muon flux is increased by about 20% (1.9% by the production cross section, 14.8% by the pion, and 3.1% by the kaon production tuning).

7.2. Systematic error on the flux prediction

The systematic error on the muon flux prediction originates from uncertainty in the hadron production and measurement error of the proton beam, horn current, and alignment of the target.

7.2.1. Uncertainty in the hadron production

The systematic error on the production cross section is dominated by the uncertainty of the quasi-elastic subtraction. This assumption is based on discrepancies in the production cross section data among data sets [9].

The systematic error of the pion or kaon differential production comes from:

(1) measurement error of the pion/kaon differential production,
(2) uncertainty in the momentum or target scaling,
(3) uncertainty from the pion/kaon production in the phase space not covered by data.

In addition to the uncertainties listed above, the systematic error on the muon flux also arises from uncertainty in secondary nucleon production. The error is primarily estimated using other experimental data sets [19,20]. For the region where the incident protons undergo a small momentum transfer, we assign 100% error to the production due to the lack of relevant data.

The muon flux is produced by the decay of the mesons which are generated at the beam dump (C) and this contributes about 4% of the total flux, as shown in Table 5. We have not corrected the hadronic interaction at the beam dump because of the small contribution to the total interactions. When it is corrected, it results in a decrease of the muon flux by 0.7%. The change of 0.7% is assigned to the systematic error on the muon flux.

The muon flux is also generated from decays of Λ, Σ, or other particles whose productions are not corrected. According to the MC simulation, 0.6% of the muons come from such particles. Since there is no relevant data for such production, we conservatively assign a 100% error to the production in these cases. In addition, 0.6% of muons come from decays of quaternary particles, which are not corrected at this stage because of the small contributions to the muon flux. A 100% error is conservatively assigned in this case.

In total, we attribute 13.4% of the systematic error in the muon flux to uncertainty in the hadron production and summarize those errors in Table 12.

to the 2007 data and phase space coverage was enlarged. Therefore the flux is expected to be predicted more precisely with the 2009 data.

Table 12. Systematic errors on the muon flux due to uncertainty in the hadron production.

Error source	Error size
Pion production	9.0%
Kaon production	1.3%
Production cross section	9.1%
Secondary nucleon production	3.6%
Dump interaction	0.7%
Decays from Λ, Σ, and quaternary particles	1.2%
Total	13.4%

7.2.2. Uncertainty in the proton beam measurement

The trajectory and optics of the proton beam are measured by the proton beam monitors placed in the primary beam line as described in Sect. 2. In the MC simulation, the parameters of the proton beam are varied within those errors attributed to the measurement errors from the proton beam monitors. The resultant variation of the muon flux (0.9%) is then estimated at the muon monitor and is taken as the systematic error on the muon flux.

7.2.3. Uncertainty in the absolute horn current

During beam operation, the monitored values of the horn current were found to drift by up to 2%, 5 kA. The drift is considered to be mainly due to the temperature dependence in the hardware monitoring. In the MC simulation, the horn currents are varied by 5 kA from the nominal values ($= 250$ kA). The variation of the muon flux, 3.6%, is then taken as the systematic error on the muon flux.

7.2.4. Uncertainty in the target alignment

The rotation of the target with respect to the horn-axis was surveyed and was measured to be 1.3 mrad (0.1 mrad) in the horizontal (vertical) direction. The effect of the target alignment is estimated by rotating the target in the simulation according to the measured values described above. The resultant variation of the muon flux, 0.5%, is assigned to the systematic error.

7.2.5. Skin effect in the magnetic horns

Since the horn current is applied as pulses of about 1 ms, the current would flow only around the surface of the conductor due to the skin effect. However, the present MC simulation assumes a flat current density. To estimate the size of the skin effect, the magnetic field in the simulation is modified by taking the skin depth into account. The modification results in decreasing the muon flux by 2.0%. The change is assigned to an additional systematic error.

7.2.6. Summary of the systematic error on the absolute muon flux

Table 13 summarizes the systematic error on the absolute muon flux prediction. Finally, we assigned a total of 14.1% error to the absolute muon flux. In the case of 0 kA horn current setting, the systematic error cannot be fully evaluated because the phase space of pions (kaons) is poorly covered by data. This may result in a large error size for the muon flux. From these reasons, we evaluated the systematic error only for the 250 kA operation.

Table 13. Summary of the systematic error on the absolute muon flux.

Error source	Error size
Hadron production	13.4%
Proton beam	0.9%
Absolute horn current	3.6%
Target alignment	0.5%
Horn skin effect	2.0%
MC statistics	0.3%
Total	14.1%

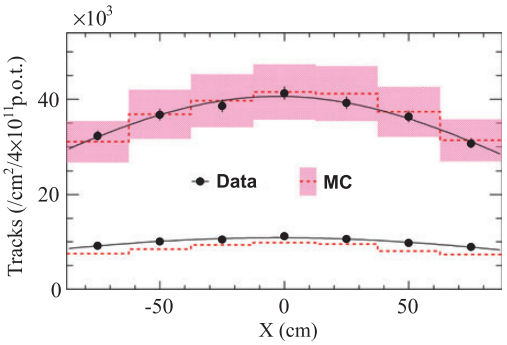

Fig. 28. Comparison of the reconstructed fluxes at the emulsion between the measurement and prediction for 250 kA (top) and 0 kA (bottom) operation. The error band represents the uncertainty of the flux prediction at 250 kA and is not drawn for the prediction at 0 kA.

Table 14. Comparison of the reconstructed flux at the emulsion detector between measurement and prediction. The fluxes are normalized to 4×10^{11} p.o.t. For the measured flux, the first error is due to the statistical error and the systematic uncertainty of each module and the second one comes from the 2.6% systematic uncertainty of the p.o.t. measurement.

	0 kA			250 kA		
	Flux tracks cm^{-2}	Flux ratio (Data/MC)	Fitted profile width (cm)	Flux tracks cm^{-2}	Flux ratio (Data/MC)	Fitted profile width (cm)
Data	$10892 \pm 126 \pm 283$	—	122.4 ± 6.5	$40628 \pm 468 \pm 1056$	—	105.6 ± 4.1
T2K MC	9682	1.12	100.3	41833	0.971	98.7

7.3. Comparison with the emulsion measurement

Figure 28 and Table 14 show the comparison between the measurement and prediction for the reconstructed profile of the muon flux at the emulsion detector, where the hadron production is corrected as described in Sect. 7.1. In the case of 250 kA operation, the ratio of the measured muon flux to the prediction is 0.97 ± 0.14. The data and prediction agree quite well. In case of 0 kA operation, there is about a 10% discrepancy in the flux between the measurement and prediction. This is because the phase space of secondary pions contributing to the muon flux at the emulsion is less constrained by the external data. This result demonstrates that our understanding of the muon, and hence neutrino, production is quite good for the 250 kA horn setting.

8. Conclusion

In this paper, we described the measurement of the beam direction by the muon monitor and the study of the muon yields with the emulsion detector. The systematic error of the beam direction measurement with the muon monitor was estimated to be 0.28 mrad and fulfills our requirement of < 0.3 mrad. The muon monitor performs the spill-by-spill measurement of the muon beam with good resolution, which enables us to keep the beam stable and control the direction within 0.3 mrad for most of the span of beam operation. Thus, the neutrino beam direction has also been kept stable within 0.3 mrad and this was, indeed, confirmed by the INGRID measurement. These beam measurements provided by the muon monitor have guaranteed good quality beam data for use as an input to the neutrino oscillation measurements. The muon monitor has also played an important role in surveying the configuration of the beamline components. To confirm our understanding of the muon and neutrino beams, the absolute muon flux was measured with the emulsion detector with a precision of 3%. It was then compared with prediction based on external hadron interaction data. As a result, we obtained good agreement between the data and prediction. This result supports our understanding of the detector performance of the muon monitor and confirms the validity of the beam control by the muon monitor.

Acknowledgements

We thank the J-PARC staff for superb accelerator performance and the CERN NA61 collaboration for providing valuable particle production data. We also would like to thank the J-PARC neutrino beam group for their great efforts in producing high-quality beam data and the Nagoya University for helping us with the emulsion detector construction. We acknowledge the support of MEXT, Japan, and SNSF and the Canton of Bern, Switzerland. In addition, authors have been further supported by funds from JSPS, Japan.

References

[1] K. Abe et al. (T2K Collaboration), Nucl. Instrum. Meth. **A659**, 106 (2011).
[2] K. Matsuoka et al., Nucl. Instrum. Meth. **A624**, 591 (2010).
[3] A. K. Ichikawa, Nucl. Instrum. Meth. **A690**, 27 (2012).
[4] K. Abe et al. (T2K Collaboration), Nucl. Instrum. Meth. **A694**, 211 (2012).
[5] S. J. Harris and C. E. Doust, Radiat. Res. **66**, 11 (1976).
[6] H. J. Ziock et al., IEEE Trans. Nucl. Sci. **40**, 344 (1993).
[7] T. Higuchi et al., [arXiv:hep-ex/0305088] [Search INSPIRE].
[8] A. Ferrari et al., CERN-2005-010 (2005).
[9] K. Abe et al. (T2K Collaboration), Phys. Rev. D **87**, 012001 (2013).
[10] R. Brun, F. Carminati, and S. Giani, CERN-W5013 (1994).
[11] C. Zeitnitz and T. A. Gabriel, In Proc. Int. Conf. on Calorimetry in High Energy Physics 1993.
[12] S. Bhadra et al., Nucl. Instrum. Meth. **A703**, 45 (2013).
[13] T. Nakamura et al., Nucl. Instrum. Meth. **A556**, 80 (2006).
[14] N. Armenise et al., Nucl. Instrum. Meth. **A551**, 261 (2005).
[15] V. Tioukov et al., Nucl. Instrum. Meth. **A559**, 103 (2006).
[16] N. Abgrall et al. (NA61/SHINE Collaboration), JINST **9**, P06005 (2014).
[17] N. Abgrall et al. (NA61/SHINE Collaboration), Phys. Rev. C **84**, 034604 (2011).
[18] N. Abgrall et al. (NA61/SHINE Collaboration), Phys. Rev. C **85**, 035210 (2012).
[19] T. Eichten Nucl. Phys. **B44**, 333 (1972).
[20] J. V. Allaby et al., Technical Report 70-12, CERN (1970).
[21] I. Chemakin et al., Phys. Rev. C **77**, 015209 (2008).
[22] G. Bellettini et al., Nucl. Phys. **79**, 609 (1966).
[23] R. P. Feynman, Phys. Rev. Lett. **23**, 1415 (1969).
[24] M. Bonesini et al., Eur. Phys. J. **C20**, 13 (2001).
[25] D. S. Barton et al., Phys. Rev. D **27**, 2580 (1983).
[26] P. Skubic et al., Phys. Rev. D **18**, 3115 (1978).